4. Laser perturbation of the discharge.

One of the drawbacks of the method of optical absorption is that it is impossible to avoid perturbation of the excited state number densities by the light source. It is crucial to determine the extent to which this occurs, for two reasons. Firstly, this affects the relationship between the number density of these states and the amount of light absorbed. The second reason arises because the optical 'pumping' causes the concentration of metastables to decay at a rate which is greater than the free decay rate; the pumping rate must therefore be known if the latter is to be determined accurately.

In this chapter the relationship between the light intensity and the pumping rate is discussed. The analysis is broken into three parts. The energy level scheme of the argon atom is discussed in section 4.1, with a particular emphasis upon the coupling between the four 1s levels and the effect this has on the subsequent analysis. In section 4.2, the relationship between the optical pumping rate and the laser intensity is examined. Saturated absorption in an inhomogeneously broadened transition is discussed and a general expression relating the absorption coefficient to the laser intensity is derived. In section 4.2.2, this expression is modified to accommodate the highly localised nature of the laser radiation used in the present study. It is shown that the onset of saturation of the absorption coefficient is in each case given by an expression of the same form. The final section addresses the increase in the rate of free decay of the concentration of metastables due to the laser radiation. It is shown that the narrowness of the beam imposes a severe limit upon the maximum perturbation of the decay rate.

4.1. Energy levels and collisional coupling in argon.

The purpose of this section is to demonstrate that collisional coupling between closely spaced excited states of the argon atom can be neglected for the most part when attempting to calculate the extent of the perturbation due to laser irradiation. This allows the entire system of energy levels to be approximated by just three: the ground state and the upper and lower states of the transition of interest.

A portion of the argon energy level diagram is displayed in figure 4.1. Paschen notation has been used to label the states. The $1s_3$ and $1s_5$ states are unable to decay to the ground state by the emission of dipole radiation and are therefore metastable, with

radiative lifetimes on the order of seconds (Small-Warren and Lue-Yung 1975). The other two states are strongly coupled to the ground state and, at pressures of greater than about 1 Torr, their resonant radiation is significantly 'trapped' (Ellis and Twiddy 1969 and Copley and Lee 1975). These two states might therefore be present in the discharge at detectable concentrations. However, measurements of their concentrations have not been attempted during the present study.

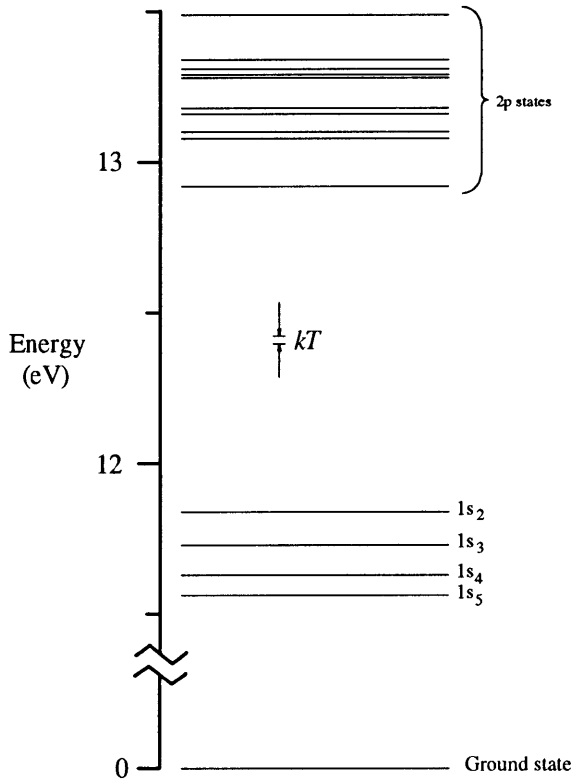

Figure 4.1. The 1s and 2p levels of the argon atom.

From figure 4.1 it can be seen that the 1s states are separated by energies on the order of three to four times kT at room temperature (k being Boltzmann's constant and T the temperature in kelvin). The degree to which these states are coupled by collisions with ground state atoms might therefore be expected to be small, but perhaps not negligible. It is therefore desirable to examine the rates involved in more detail. This is done below for three different situations: (i) the free decay in the absence of laser perturbation; (ii) the steady-state discharge, again in the absence of laser perturbation; (iii) the steady-state discharge, including the effects of laser perturbation.

4.1.1. Free decay, no laser perturbation.

The metastable $1s_3$ and $1s_5$ states obey the rate equations

$$\frac{\partial N_i}{\partial t} = D_i \nabla^2 N_i - G_i N_i + \varepsilon_i(\mathbf{r}) + N_0 \sum_{j \neq i} C_{ji} N_j , \qquad j = 2 \text{ to } 5 \tag{4.1}$$

where N_i, D_i, G_i and ε_i are respectively the concentration, diffusion coefficient, volume quenching coefficient and rate of generation of state i, N_0 is the concentration of ground state atoms and $N_0 C_{ij}$ is the rate at which atoms in state i are converted to state j by collision with a ground state atom. Paschen's numbers for the 1s levels have been used for the indices i and j. Equation (4.1) is identical to equation (2.14), except that the form of the generating function ε_i has been left implicit; some different symbols have also been used, for reasons of internal consistency within the present chapter. The two resonant states obey an equation similar to equation (4.1), except that the diffusion term must be replaced by a term describing the quasi-diffusive escape of the resonance radiation. Holstein (1947) showed that this relaxation mechanism could be modelled as a sum of different decay modes. The decay rate $\nu_{i,1}$ of the dominant mode within an infinite parallel plane geometry is given by

$$\nu_{i,1} \sim \frac{3}{2\tau_i k(0) d \sqrt{\ln[k(0)d]}} \tag{4.2}$$

where d is the separation of the planes and $k(0)$ is the line-centre absorption coefficient. The free decay of these levels will not be discussed further as their rates of decay are too fast to measure with the equipment available.

The volume quenching coefficient G_i arises from a combination of a number of processes (Phelps 1959, Ellis and Twiddy 1969) and may be expanded as

$$G_i = \nu_{\text{imp}} + \frac{1}{\tau_i} + N_0 \sum_{j \neq i} C_{ij} + N_0^2 F_i . \tag{4.3}$$

This equation is identical, apart from notation, to equation (3.43). The explanation of the four terms is as follows:

ν_{imp} - The rate of destruction by collision with impurity particles.

$1/\tau_i$ - The rate of radiative decay to the ground state (by the electric quadrupole or magnetic dipole mechanisms, in the case of metastable particles). These rates are negligible (Small-Warren and Lue-Yung 1975).

$N_0 C_{ij}$ - As in equation (4.1), this is the rate of conversion to state j by collision with a single ground-state atom.

$N_0^2 F_i$ - The rate of three-body reactions of the form

$$Ar^* + Ar + Ar \rightarrow Ar_2^* + Ar + K.E.$$

The creation and decay channels of such dimers have been discussed by many authors (eg. Boucique and Mortier 1970, Thonnard and Hurst 1972, Wieme and Wieme-Lenaerts 1974, Birot *et al* 1975 and Wieme and Lenaerts 1981). More recently Manzanares and Firestone (1983) have shown that a decay mechanism involving a collisional-radiative cascade down the vibrational levels of the excimer may be the source of first-order term in equation (4.3), rather than an actual two-body collision.

Other mechanisms exist but they have been found to be of no importance within the discharge regimes which were used in the present study.

The coefficients C_{ji} and C_{ij} can be related by use of the principle of detailed balance, giving:

$$\frac{C_{ji}}{C_{ij}} = \frac{g_i}{g_j} \exp\left(\frac{E_j - E_i}{kT}\right) \tag{4.4}$$

where g_i and E_i are respectively the statistical weight and energy of the ith state. Values (where known) of the F_i and C_{ij} coefficients for the four 1s states of argon are given in tables 4.1 and 4.3; the ratios between the C_{ij} coefficients are listed in table 4.2. These tables can be found at the end of the chapter, on pages 94 and 95.

A detailed discussion of the influence of collisional coupling among the 1s levels during the free decay can be found in Ellis and Twiddy (1969). These authors found that the population and coefficient ratios in argon were such that the sum over $C_{ji}N_j$ could be neglected when state i is one of the two metastable states. Collisional transfer from the $1s_4$ and $1s_2$ states to the $1s_5$ or $1s_3$ states was found to be negligible because the

concentrations of these states decreased rapidly to very small values during the free decay. Ellis and Twiddy found the concentration N_5 of the $1s_5$ state to be about 100 times larger than N_3. Since the ratio between C_{53} and C_{35} is about 10^{-4}, this implies that $C_{53}N_5 \sim 10^{-2}$ $C_{35}N_3$. The transfer from $1s_5$ to $1s_3$ therefore has very little influence on the $1s_3$ concentration and can be neglected. The rate of transfer the other way is, of course, much larger; it is, in fact, of the order of 12 atoms s^{-1} at 1 Torr gas pressure. The minimum possible value of ν_5, the total rate of decay rate of the $1s_5$ states, occurs in the present apparatus at about this pressure and is about 90 atoms s^{-1}. Therefore the transfer of atoms from the $1s_3$ to the $1s_5$ state can be neglected, at least to first order, when calculating the evolution of the latter.

4.1.2. Steady state, no laser perturbation.

This arrangement corresponds approximately to the experiment of Tachibana* (1986). This author found that the ratio between the $1s_5$ and $1s_3$ states was approximately the same as in the free decay case, but the concentrations of the $1s_4$ and $1s_2$ states were much greater, although still an order of magnitude or two below the concentrations of the metastable states. A consideration of the energy separations between the states and of equation (4.4) indicates that significant transfer can occur at these concentrations only by the pathways $1s_2 \rightarrow 1s_3$, $1s_4 \rightarrow 1s_5$, $1s_3 \rightarrow 1s_4$ and $1s_5 \rightarrow 1s_4$. It is not possible to show that the last two can be safely neglected, but a rigorous analysis of the expected steady-state distributions of the $1s_2$ and $1s_4$ states has not been attempted here in any case. The other two processes would have manifested in Tachibana's experiment as a pressure-dependence in the measured value of the reduced excitation coefficients α_3/N_0 and α_5/N_0. Tachibana measured both these coefficients over a pressure range of about 0.3 to 3 Torr (while keeping the reduced electric field E/N_0 constant), but found no detectable variation within the experimental error of about 15%. Hence it can be concluded that the rates $N_0C_{23}N_2$ and $N_0C_{45}N_4$ are insignificant in this regime as well.

---

* This author employed a laser absorption technique to measure the concentrations of excited states, but the radiation was spread out spatially and therefore of much lower intensity than is the case in the present study. Such weak irradiation perturbs the system very little and can, to a first approximation, be ignored.

4.1.3. Laser perturbation of the steady-state discharge.

It has been shown above that the influence of the other 1s levels upon the concentrations of the metastable $1s_3$ and $1s_5$ states can be neglected in the absence of any other effects, but the situation is a little different when a transition between a 1s and a 2p state is perturbed by intense laser radiation. The depletion of the lower level by optical pumping is partially offset by radiative decay of the upper level; other 1s states can complicate the picture if there is more than one significant pathway for the decay of the 2p state. Such a situation is illustrated in figure 4.2.

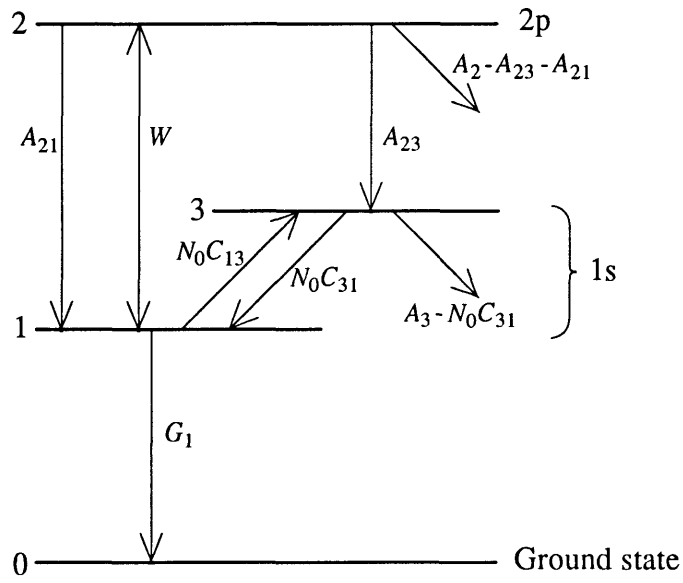

Figure 4.2. Possible paths of transfer between levels and their symbols.

It was therefore necessary to show that indirect decay of the 2p atoms via other 1s states could be neglected for the transitions of interest. This was done by calculating the fractional excess $\delta_2\delta_3$ in the rate of decay of the upper to the lower state due to such 'sideways' decay processes. This quantity may be approximated by the following product of branching ratios:

$$\delta_2\delta_3 \sim \frac{A_{23}}{A_2} \times \frac{N_0C_{31}}{A_3}. \qquad (4.5)$$

The coefficient A_i is here the total rate of decay (ie, radiative plus collisional) of state i. The quantity $\delta_2\delta_3$ is calculated below for each transition that was examined in the course

of this study. Only 5 of the 30 allowed 1s - 2p transitions were studied.* Some of those for which measurements were not attempted are too weak to yield a measurable absorption signal; others are outside the tuning ranges of the available lasers.

In the following discussion, the 2p radiative branching ratios have been taken from Shumaker and Popenoe (1967), the 1s collisional coupling rates from Ellis and Twiddy (1969), the 2p collisional coupling rates from Nguyen and Sadeghi (1978) and the lifetimes of the resonant $1s_2$ and $1s_4$ states from Lawrence (1968).

$1s_5$ - $2p_9$, 8115 Å:

The only dipole-allowed decay of the $2p_9$ state is to the $1s_5$ state. However, decays to other 1s states can take place via collisional transitions between 2p levels. As far as the $2p_9$ state is concerned, the most significant result of this collisional mixing is a slight diversion of atoms into the $1s_4$ state. At one Torr, about 0.6% of the $2p_9$ atoms decay by this path. The proportions going to the other two 1s states are an order of magnitude lower. At the same pressure, the rate of collisional transfer between $1s_4$ and $1s_5$ has been determined to be less than 1000 s^{-1}, whereas the total decay rate of the $1s_4$ state is about 3 x 10^4 s^{-1}. The fractional excess in A_{21} due to collisional mixing is therefore given by equation (4.5) as 0.017%, far smaller than the uncertainty in A_{21}.

$1s_4$ - $2p_5$, 7515 Å:

The electric dipole selection rules impose similar restrictions upon this transition. Collisional transitions among 2p states lead to 0.9% of $2p_5$ atoms decaying to the $1s_5$ state and 0.3% to the $1s_3$ state at 1 Torr. Unfortunately the available data do not allow the ratio N_0C_{31}/A_3 to be deduced for either $1s_5$ or $1s_3$. However, since the ratio cannot be greater than unity, the total $\delta_2\delta_3$ must in any case be less than 1.2% and is therefore negligible.

$1s_4$ - $2p_7$, 8104 Å:

15% of the $2p_7$ atoms decay to the $1s_5$ state and 7.5% to the $1s_3$ state. Although it is, once again, not possible to quantify the branching ratios of the $1s_5$ and $1s_3$ decays, most

*Although only $1s_5$ - $2p_9$ measurements are reported in chapter 10, it is intended to investigate some of the other four transitions in the near future.

of these atoms probably end up in the $1s_4$ state. This is the most energetically favourable route for the two-body collisional transition of $1s_5$; the next nearest state, the $1s_3$, lies 3.8 *kT* further 'uphill'. The only other significant decay mechanism for the $1s_5$ is via collision with two ground state atoms to produce the excimer Ar_2^*. For the $1s_5$ state, the rate of this process is smaller than the two-body rate at pressures below about 1.6 Torr. Similar considerations apply to the decay of the $1s_3$ state. It seems, therefore, that the effects of collisional coupling among 1s states cannot be ignored for this transition, in the absence of any other consideration. However, the absorption experiments described here employed a narrow beam of laser radiation. At 1 Torr, the total rate of transfer from $1s_5$ to $1s_4$ is 33 s^{-1} and the rate from $1s_3$ to $1s_4$ must be less than 190 s^{-1}; since these rates are less than the respective values of D/Λ^2 for the states (Λ here is roughly equal to the beam diameter of ~1 mm), atoms in these states are likely to diffuse out of the beam before transferring to the $1s_4$ state. Because of this, it is considered that, for present purposes at least, collisional interactions can be neglected for this transition as well.

$1s_3$ - $2p_2$, 7724 Å:

44% of the $2p_2$ state decays to the $1s_2$, 5% to the $1s_4$ and 18% to the $1s_5$. From the values for A_3 and N_0C_{31} listed in table 4.3, the total $\delta_2\delta_3$ may be calculated to be less than 0.16%, a negligible value.

$1s_2$ - $2p_1$, 7505 Å:

The $2p_1$ state is strongly coupled to the $1s_2$, only 0.5% decaying by the alternative route to the $1s_4$ state. The analysis ought therefore to be similar to that for the $1s_5$ - $2p_9$ transition, except that the effect is probably even smaller because transfers from the low to high levels are less energetically favourable than vice versa.

The conclusion of these individual analyses is that all the transitions that were studied can be modelled as three level systems for the purposes of calculation of the laser perturbation (within a narrow beam, at least).

4.2. The absorption coefficient, and new results concerning saturation of the absorption under the present experimental conditions.

4.2.0. Introduction.

In order to deduce the number densities of excited argon atoms from the amount of light they absorb from a beam of laser radiation, it is necessary to arrive at an expression for the absorption coefficient. There are several features of the present experimental arrangement which complicate this undertaking. These are discussed immediately below.

(i) The 1s - 2p transitions in argon at about 1 Torr and 300 K are inhomogeneously broadened. The light source used by the author is a GaAlAs semiconductor junction laser; the bandwidths of these devices are typically in the tens of MHz (Takakura *et al* 1980, Okoshi *et al* 1980 and Saito and Yamamoto 1981), several orders of magnitude below the Doppler transition width of about 1 GHz. The narrow bandwidth of the laser means that the laser radiation does not couple to all the atoms in the state of interest with the same strength. To see this, suppose that the centre frequency f_L of the intensity envelope $I(f)$ of the laser is tuned to coincide with the centre frequency f_T of the transition. Atoms in the lower state of the transition that are neither approaching or receding from the light source will be strongly coupled to the radiation field. Atoms moving away from the light source at a speed v_z will, however, experience a radiation field with a Doppler-shifted central frequency f' given by

$$f' = f_L(1 - v_z/c). \tag{4.6}$$

If their velocity is such that $|f' - f_T| > \Delta f_H$, where Δf_H is the homogeneously broadened linewidth, the coupling of these atoms to the radiation field will be much weaker. A simple calculation shows that most argon atoms may be expected to have velocities outside this range at room temperature. A rigorous calculation of the absorption coefficient must therefore be performed by first calculating the effect of the laser on a subset of excited atoms with components of velocity in the direction of propagation of the radiation which fall within a narrow interval. The net perturbation may then be deduced by integration over all the velocity subsets.

(ii) In order to resolve the spatial structure of the distribution of absorption by excited states, a narrow beam of radiation has been used in the present study. This factor, together with the narrow bandwidth of the laser, means that the intensity of the radiation

per unit frequency interval is high (possibly as much as 100 μW Hz^{-1} m^{-2}, corresponding to an effective temperature of 200,000 K). Saturation of the transition cannot be neglected under these conditions. This issue is addressed with some care in the present section.

(iii) The non-uniform illumination of the discharge introduces a spatial dependence into the rate equations which describe the distribution of the states under the influence of the radiation. The geometry which is most convenient from an experimental point of view, namely a beam propagating in the x direction in a discharge which has a cylindrical symmetry about the z axis, is resistant to simple mathematical attack. For this reason, the absorption coefficient has been calculated in the present section for two simpler models: an infinite steady-state discharge illuminated by a uniform intensity of radiation, and the same discharge illuminated by a thin beam of circular cross-section. The resulting expressions are found to be identical apart from a scaling factor in the onset of saturation. This suggests that the variations that are imposed by an awkward geometry may be of a similar nature and are perhaps best addressed empirically.

4.2.1. Steady state, uniform discharge perturbed by spatially uniform laser light.

An expression relating the absorption coefficient to the laser intensity is derived in this section under the assumption that none of the discharge or laser parameters has any spatial variation. As shown above, the system of energy levels of the argon atom can be approximated by a three level system, the levels being labelled 0 to 2 for generality. In this scheme state 0 represents the ground state, state 1 the 1s level that is being measured and state 2 the 2p state that is coupled to state 1 by the laser radiation. It is assumed that N_2 and N_1 are much smaller than N_0, which is assumed to be constant. This is a realistic approximation within a weak discharge where level 1 is metastable.

As mentioned in the introduction to section 4.2, it is necessary to consider separately the effect of the radiation upon atoms in different velocity classes. If the radiation propagates in the z direction, the rate of increase in the population of atoms with a z-component of velocity between v_z and $v_z + dv_z$ is given by

$$\frac{\partial n_i}{\partial t} dv_z = \left\{ D_i \nabla^2 n_i + \varepsilon_i \Gamma(v_z) - \sum_{j=1}^{2} h_{ij} n_j - \left[n_i - \int dv_z' \sigma(v_z', v_z) n_i(v_z') \right] N_0 C_i(v_z) \right\} dv_z \qquad (4.7)$$

where $n_i dv_z$ is the number density of atoms in this velocity class, $N_0 C_i$ is the rate of elastic collisions between an atom in state i and a ground-state atom and $\sigma(v_z', v_z)dv_z$ is the probability that an atom with velocity between v_z' and $v_z' + dv_z$ before such a collision will have a velocity between v_z and $v_z + dv_z$ after the collision. The function Γ is the normalised Doppler profile

$$\Gamma(v_z) = \sqrt{\frac{m}{2\pi kT}} \exp\left(-\frac{mv_z^2}{2kT}\right). \tag{4.8}$$

In the above expression m is the atomic weight of argon, k is Boltzmann's constant and T the temperature. The matrix of h values is

$$\mathbf{h} = \begin{bmatrix} \frac{g_2}{g_1} w + G_1 & -w - A_{21} \\ -\frac{g_2}{g_1} w & w + A_2 \end{bmatrix} \tag{4.9}$$

where g_1 and g_2 are the statistical weights of levels 1 and 2, $w(v_z)$ is the optical pumping rate for atoms in this velocity class, G_1 is the quenching rate of the metastable level, A_{ij} is the transition rate between the ith and the jth level and $A_2 = A_{20} + A_{21}$ is the total decay rate of level 2.

For the remainder of this chapter the dv_z will be omitted from similar rate equations.

Before an attempt is made to solve the coupled equations implicit in equation (4.7), some general relationships will be derived, following the usual method. The rate at which energy is lost from the incident radiation is given by the rate of absorption minus the rate of stimulated emission. The decrease in the total intensity I in the direction of propagation is therefore given by

$$\frac{\partial I}{\partial z} = -hf \int dv \left[\frac{g_2}{g_1} n_1(v_z) - n_2(v_z)\right] w(v_z). \tag{4.10}$$

(Note that h in this equation represents Planck's constant.) Because of the spread in atomic velocities, $w(v_z)$, the pumping rate per unit velocity interval, is given by the convolution

$$w(v_z) = \int_{-\infty}^{\infty} df\, I(f) B_{21}\, L[f - f_0(v_z)] \tag{4.11}$$

where B_{21}, the Einstein coefficient for stimulated emission, is given for the case of linearly polarised radiation incident upon a population of unaligned atoms by (Siegmann 1986)

$$B_{21} = \frac{A_{21}\lambda^3}{8\pi hc} \tag{4.12}$$

and L is the normalised Lorentzian lineshape

$$L(f) = \frac{\Delta f_H}{2\pi\left\{f^2 + (\Delta f_H/2)^2\right\}}. \tag{4.13}$$

The quantity

$$f_0(v_z) = f_T\left(1 + \frac{v_z}{c}\right) \tag{4.13a}$$

is the Doppler-shifted frequency of the transition centre for atoms moving away from the light source at speed v_z, as measured in the laboratory frame of reference. The homogeneously broadened linewidth Δf_H is given by

$$\Delta f_H = (A_{21} + 2\eta)/2\pi, \tag{4.14}$$

where η is the pressure broadening coefficient. The integral in equation (4.11) may be approximated if the laser linewidth Δf_L is much narrower than the homogeneous linewidth Δf_H (a reasonable assumption in the present case) giving

$$w(v_z) \sim I B_{21}\, L[f_L - f_0(v_z)] \tag{4.15}$$

where f_L is the centre frequency of the laser line.

It was necessary to modulate the wavelength of the laser as part of the feedback mechanism for keeping the laser wavelength near to the centre of the atomic transition (see chapter 7 for details). However, because the frequency of modulation is two to three orders of magnitude slower than the natural decay rates of the 1s - 2p transitions, the laser

output wavelength may be considered to be constant to a good approximation over the natural time scale of the transition processes.

Having arrived at an expression for the optical pumping rate for atoms with velocity component between v_z and $v_z + dv_z$, the form of the absorption coefficient k can be deduced. Substitution of equation (4.15) into equation (4.10) gives

$$\frac{\partial I}{\partial z} = -kI(z) \tag{4.16}$$

where

$$k \sim hfB_{21}\int dv_z \left[\frac{g_2}{g_1} n_1(v_z) - n_2(v_z)\right] L[f - f_0(v_z)]. \tag{4.17}$$

4.2.1.0. The weak-field limit.

An expression for k_0, the absorption coefficient in the weak radiation limit, can be derived as follows. If the laser perturbation is small, the concentrations n_1 and n_2 of states 1 and 2 per unit velocity interval may be approximated by their values when the perturbation is zero. These values are given by

$$n_{i,0}(v_z) = N_{i,0}\Gamma(v_z) \tag{4.18}$$

where $N_{i,0}$ is the total concentration of the state i in the absence of laser perturbation. If the homogeneous linewidth Δf_H is significantly smaller than the Doppler linewidth Δf_D, then the concentrations n_1 and n_2 in equation (4.17) will be slowly varying functions of v_z over the interval where the lineshape L is significant; this is the case within the ranges of pressure and temperature used in the present experiments. Equation (4.17) may therefore be approximated in the small-signal limit by

$$k_0 \sim hB_{21}c\,\Delta N_0\,\Gamma(v_{z,0}) \tag{4.19}$$

where

$$\Delta N = \frac{g_2}{g_1} N_1 - N_2 \tag{4.20}$$

and

$$v_{z,0} = c\left(\frac{f_L}{f_T} - 1\right). \tag{4.21}$$

The optical cross-section $\sigma = k/\Delta N$ provides a measure of the strength of the absorption which is independent of the concentration of states 1 or 2. Small-signal values of σ for the lines of interest are listed in table 4.4 on page 95.

As mentioned in the introduction to section 4.2, saturation of the transition is likely to be of importance under the present experimental conditions because of the narrowness of the laser radiation in both spatial dimension and frequency (1.6 mm diameter and 10 MHz respectively). Many authors have discussed saturation of gain or absorption in an inhomogeneously broadened transition in the context of laser resonators (eg Bennett 1961, Szöke and Javan 1963, Lamb 1964, Gyorffy *et al* 1968, Cordover and Bonczyk 1969, Greenstein 1972 and Shirley 1973). The physical situation inside a laser resonator is, however, somewhat more complicated than is the case in the simple absorption experiment described here. This is because, in a laser resonator, both the radiation and the population of emitting and absorbing atoms are inside a (nearly) closed feedback loop and must therefore arrive at a mutual equilibrium. A workable theory of saturation of gain in a laser resonator must, for example, treat the variation in refractive index of the gas that is induced by the radiation field as well as the induced changes in the absorption coefficient, together with the effects these parameters have upon the radiation field. The theoretical treatments of the above authors are thus very complete, but unnecessarily complicated for use in the present case. On the other hand, most textbooks on spectroscopy contain an elementary discussion of saturated absorption in an inhomogeneously broadened transition. A typical discussion of the saturation relation at this level is reproduced in section 4.2.1.1. These 'textbook' treatments tend to suffer from the opposite problem, being a little too simple to be useable in a broad range of situations. In particular, few textbooks mention the effect of collisional redistribution of atoms among velocity classes (also known as 'cross-relaxation'), which may not be negligible at the pressures used in the experiments described here. Because the available theory seems to fall between two stools, as it were, an attempt has been made in section 4.2.1.2 to extend the simple 'textbook' theory to the case where the effects of collisional redistribution are not negligible.

4.2.1.1. Saturation of absorption in the absence of cross-relaxation.

In this limit, the C_i in equation (4.7) can be set to zero. In a steady state, uniform discharge, the time and space derivatives are zero as well. The result can be expressed in matrix form as

$$\sum_{j=1}^{2} h_{ij} n_j = \varepsilon_i \Gamma, \quad i = 1, 2. \tag{4.22}$$

The remainder of the analysis of this limiting case follows Yariv (1976) fairly closely. The population inversion parameter Δn can be found by solving equation (4.22), giving

$$\Delta n = \frac{\Delta N_0 \Gamma}{1 + w\Omega / A_{21}} \tag{4.23}$$

where

$$\Omega = \delta \left[1 + \frac{g_2}{g_1} \frac{A_{20}}{G_1} \right] \tag{4.24}$$

and δ is the branching ratio

$$\delta = \frac{A_{21}}{A_2}. \tag{4.25}$$

Insertion of equations (4.23), (4.12) and (4.13) into equation (4.17) gives

$$k = \frac{\Delta N_0 A_{21} \lambda_T^4 \Delta f_H}{16\pi^2} \int_{-\infty}^{\infty} \frac{\Gamma(v_z) dv_z}{(v_z - v_{z,0})^2 + \lambda_T^2 \left(\frac{\Delta f_H}{2} \right)^2 + \frac{\Omega \lambda_T^5 I \Delta f_H}{16\pi^2 hc}}. \tag{4.26}$$

If, as has already been assumed, the Doppler width Δf_D is much larger than the homogeneous linewidth Δf_H, the Gaussian function Γ is slowly varying compared to the remainder of the integrand and may therefore be moved outside the integral without significant error in the result. The integral that remains is of the form

$$\int_{-\infty}^{\infty} \frac{dx}{x^2 + a^2}$$

where a is a constant. The solution to this integral is given in standard tables as π/a. The final result is therefore

$$k = \frac{k_0}{\sqrt{1 + I/I_{sat}}} \tag{4.27}$$

where

$$I_{sat} = \frac{4\pi^2 hc\Delta f_H}{\Omega\lambda_T^3} \tag{4.28}$$

is the saturation intensity.

4.2.1.2. Saturation of absorption in the case of significant cross-relaxation.

Consider now the case in which the cross-relaxation of atoms between velocity classes is not negligible. It is difficult to judge the quantitative effects of cross-relaxation. On the one hand, a consideration of the differential scattering cross-sections for elastic collisions between metastable excited atoms and their ground states (eg Brutschy and Haberland 1979, Beyer and Haberland 1984 and Feron *et al* 1989) seems to indicate that the probability density $\sigma(v_z, v_z')$ in equation (4.7) has a form that is sharply peaked about $v_z = v_z'$. On the other hand, the results of measurements of Doppler-free lineshapes in a number of gases (eg Smith and Hänsch 1971, Keil *et al* 1973, Bréchignac *et al* 1977 and 1978 and Otieno 1978) indicate that such lineshapes can be modelled quite well by a sum of a narrow Lorentzian and a broad, low Gaussian background. The Gaussian component is attributed to 'strong' or thermalising collisions, in other words, those in which the impact parameter is small. The natural rate of decay contributes to the width of the Lorentzian component, but this is broadened both by 'phase-interruption' effects as well as by 'weak' velocity-changing collisions. The contribution from the latter can be distinguished by mixed-gas experiments.

An exact treatment of the argon 1s - 2p lineshapes will not be attempted here. Instead, the limiting case in which σ is much wider than the 'hole' in $n_1(v_z)$ will be examined.

Let the half width at half maximum of $\sigma(v_z)$ be denoted by $\Delta v_{z,C} = c\Delta f_C / f_T$. The assumption that $\Delta f_C << \Delta f_H$ is implicit in the analysis of the preceding sub-section. In the opposite limit, $\Delta f_C >> \Delta f_H$, with the effect that the integrand in equation (4.7) is approximately constant over the range of v_z in which atoms are significantly perturbed by the laser radiation. A further simplification may be made if, at the same time, $\Delta f_C << \Delta f_D$. If this is the case, the approximation

$$C_i \int dv_z' \, \sigma(v_z', v_z) n_i(v_z') \sim C_i n_{i,0}(v_z) \tag{4.29}$$

may be used without significant error. Figure 4.3 shows qualitatively how σ and n_1 might appear if the above assumptions were true.

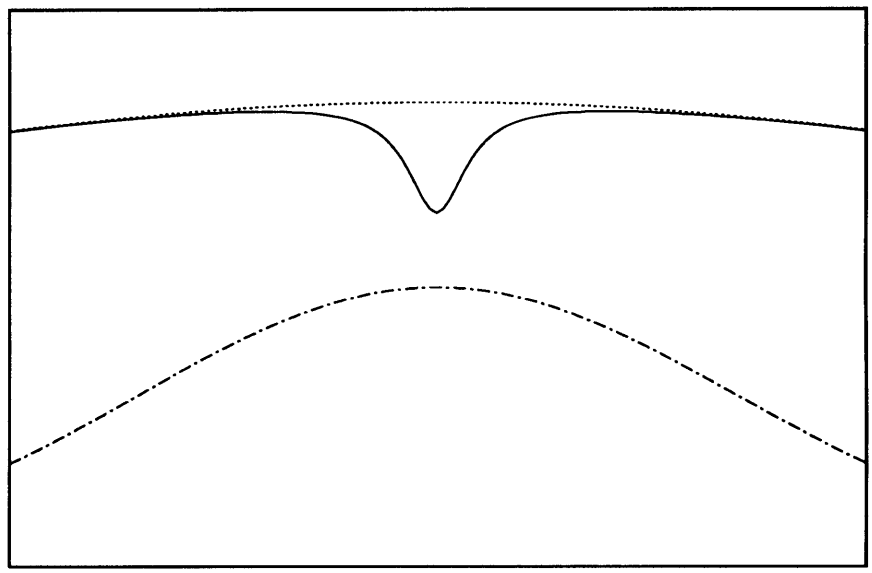

v_z (arbitrary units).

Figure 4.3. A diagram showing, schematically, the relationship between the unperturbed, thermally-broadened distribution of atoms $N_{1,0}\Gamma(v_z)$ (dotted line), the laser-perturbed distribution $n_1(v_z)$ (solid line) and the collisional redistribution cross-section $\sigma(v_z)$ which is assumed in section 4.2.1.2 (chained line). The width of the 'hole' in $n_1(v_z)$ is approximately equal to c/f_T times the homogeneous linewidth Δf_H, provided the laser linewidth Δf_L is much smaller than Δf_H. The respective half-widths at half-maximum of the unperturbed profile, the cross-section and the hole are here in the (arbitrarily chosen) ratio 20:5:1.

The rate equations in this case can be written as

$$\sum_{j=1}^{2} h_{ij} n_j = \varepsilon_i \Gamma + N_0 C_i \left(n_{i,0} - n_i \right). \tag{4.30}$$

This can be inverted and solved for Δn, giving

$$\Delta n = \frac{\Delta N_0 \Gamma}{1 + w\Omega_C / A_{21}} \tag{4.31}$$

where

$$\Omega_C = \delta_C \left[1 + \frac{g_2}{g_1} \frac{A_{20} + N_0 C_2}{G_1 + N_0 C_1} \right] \tag{4.32}$$

and

$$\delta_C = \frac{A_{21}}{A_2 + N_0 C_2}. \tag{4.33}$$

The remainder of the analysis is the same as that described above for the limit of negligible collisional redistribution. The final expression for the absorption coefficient is identical to equation (4.27), except that the saturation intensity is found by replacing Ω in equation (4.28) by Ω_C.

In the light of the above result, it seems likely that the effect of a slight collisional redistribution among states is merely to alter the value of the parameter I_{sat}, while the functional dependence between k and I remains unchanged. The correct value for I_{sat} can then be found by fitting a function of the form $(1 + I/I_{sat})^{-½}$ to experimental data. The variation in I_{sat} due to cross-relaxation may not be small. This is because the collision rate $N_0 C_i$ is likely to be of significant size at working pressures of around 1 Torr. An estimate of its value can be obtained from the approximation

$$N_0 C_i \sim \frac{\bar{v}^2}{\lambda_i} \tag{4.34}$$

where λ_i here is the mean free path between elastic collisions and $\bar{v}$ is the maxwellian mean speed (equation 3.12). By use of equation (3.20), equation (4.34) can be written

$$N_0 C_i \sim \frac{\bar{v}^2}{2D_i}. \tag{4.35}$$

For the $1s_5$ state at 1 Torr, $N_0 C_1$ works out to be about 1.6×10^7 s^{-1}, which is of similar size to the strongest of the 1s-2p transition rates. Values of $N_0 C_2$ are likely to be of similar size.

4.2.2. Steady-state, uniform discharge perturbed by a narrow beam.

In this section, the onset of saturation of the absorption coefficient will be examined for the case of a uniform field of metastable atoms which is perturbed by a narrow beam of laser radiation. The beam will be assumed to be circular in cross-section and of uniform intensity within the beam radius R_b (this is a good approximation to the actual intensity distribution - see section 7.2.2.1). In this case, the contribution of diffusion can no longer be neglected. If the beam is circular as described above, and provided the rate of decrease in the beam intensity in the direction of propagation is small, then cylindrical symmetry about the beam axis can be assumed. The spatial dependence of all quantities may then be expressed in terms of a radial coordinate r measured from beam centre. The equation describing the steady-state concentrations of states 1 and 2 per unit velocity interval can be obtained as a special case of equation (4.7):

$$\frac{D_i}{r}\frac{\partial}{\partial r}\left(r\frac{\partial n_i}{\partial r}\right)+\varepsilon_i\Gamma-\sum_{j=1}^{2}h_{ij}n_j=0. \tag{4.36}$$

The Laplacian in the diffusion term $D_i\nabla^2 n_i$ has here been expressed in cylindrical polar coordinates, with the z and ϕ derivatives set to zero.

The first step in the solution of these coupled differential equations is to convert them to a homogeneous form. This can be done by the introduction of auxiliary functions m_i. Outside the beam, where the optical pumping rate w is equal to zero, these are defined such that

$$m_i(r,v_z)=N_{i,0}\Gamma(v_z)-n_i(r,v_z). \tag{4.37}$$

The quantities $N_{1,0}$ and $N_{2,0}$ are the concentrations of states 1 and 2 in the absence of laser perturbation, and are given by

$$N_{1,0}=\frac{\varepsilon_1}{G_1}+\frac{A_{21}\varepsilon_2}{A_2G_1} \tag{4.38}$$

and

$$N_{2,0}=\varepsilon_2/A_2. \tag{4.39}$$

Use of equation (4.37) allows equation (4.36) to be expressed in the homogeneous form

$$\frac{1}{r}\frac{\partial}{\partial r}\left(r\frac{\partial m_i}{\partial r}\right)=\sum_{j=1}^{2}h'_{\text{out},ij}m_j \tag{4.40}$$

where

$$\mathbf{h}'_{\text{out}}=\begin{bmatrix}G_1/D_1 & -A_{21}/D_1\\ 0 & A_2/D_2\end{bmatrix}. \tag{4.41}$$

The equations in m_1 and m_2 can be uncoupled by use of an eigenvalue method. Let a matrix $\mathbf{Q}$ be chosen such that

$$\mathbf{Q}^{-1}\mathbf{h}'_{\text{out}}\mathbf{Q}=\Lambda \tag{4.42}$$

where Λ is a diagonal matrix of the eigenvalues λ_1 and λ_2 of $\mathbf{h}'_{\text{out}}$. Substitution of $\mathbf{y}=\mathbf{Q}^{-1}\mathbf{m}$ into equation (4.40) allows it to be transformed to the uncoupled form

$$\frac{1}{r}\frac{\partial}{\partial r}\left(r\frac{\partial \mathbf{y}}{\partial r}\right)=\Lambda\mathbf{y}. \tag{4.43}$$

Equation (4.43) has solutions

$$y_i(r)=b_iI_0\left(r\sqrt{\lambda_i}\right)+c_iK_0\left(r\sqrt{\lambda_i}\right) \tag{4.44}$$

where b_i and c_i are constants and $I_n(x)$ and $K_n(x)$ are the hyperbolic Bessel functions of order n. However, $I_0(x)$ is unbounded as x increases; the value of b_i must therefore be zero for the solution to be physically reasonable. The eigenvalues are easily shown to be

$$\lambda_1=\mu_1^2=\frac{G_1}{D_1} \tag{4.45}$$

and

$$\lambda_2=\mu_2^2=\frac{A_2}{D_2}. \tag{4.46}$$

The matrix of eigenvectors $\mathbf{Q}$ is therefore

$$\mathbf{Q}\sim\begin{bmatrix}1 & \delta D_2/D_1\\ 0 & -1\end{bmatrix}, \tag{4.47}$$

where δ is the branching ratio defined in equation (4.25). The solutions are thus found to be

$$n_1(r,v_z) = N_{1,0}\Gamma - c_1 K_0(\mu_1 r) - c_2 \frac{\delta D_2}{D_1} K_0(\mu_2 r) \tag{4.48}$$

and

$$n_2(r,v_z) = N_{2,0}\Gamma + c_2 K_0(\mu_2 r). \tag{4.49}$$

A similar approach may be pursued within the beam of radiation. Here the auxiliary functions m_i have the somewhat more complicated form

$$m_1(r,v_z) = M_{1,0}\Gamma/\Delta - n_1(r,v_z) \tag{4.50}$$

$$m_2(r,v_z) = M_{2,0}\Gamma/\Delta - n_2(r,v_z) \tag{4.51}$$

where

$$M_{1,0} = (A_2 + w)\varepsilon_1 + (A_{21} + w)\varepsilon_2, \tag{4.52}$$

$$M_{2,0} = \frac{g_2}{g_1} w\varepsilon_1 + \left(G_1 + \frac{g_2}{g_1} w\right)\varepsilon_2 \tag{4.53}$$

and

$$\Delta = G_1(A_2 + w) + A_{20}\frac{g_2}{g_1} w. \tag{4.54}$$

Equation (4.36) can be expressed in terms of these quantities as

$$\frac{1}{r}\frac{\partial}{\partial r}\left(r\frac{\partial \mathbf{m}}{\partial r}\right) = \mathbf{h}'_{\text{in}}\mathbf{m} \tag{4.55}$$

where $\mathbf{h}'_{\text{in}}$ is

$$\mathbf{h}'_{\text{in}} = \begin{bmatrix} \left(G_1 + \frac{g_2}{g_1} w\right)\Big/ D_1 & -(A_{21} + w)/D_1 \\ -\frac{g_2 w}{g_1 D_2} & (A_2 + w)/D_2 \end{bmatrix}. \tag{4.56}$$

The remainder of the analysis in the domain $r < R_b$ is similar to that used above to solve the equations in the region $r > R_b$. The expressions for the eigenvalues of $\mathbf{h}'_{\text{in}}$ are complicated and there appears to be little to be gained by reproducing them in full. However, in the limit that the optical pumping rate $w << A_2$, the eigenvalues may be approximated by

$$\lambda_1 = \mu_3^2 \sim \frac{G_1 + g_2 w(1-\delta)/g_1}{D_1} \tag{4.57}$$

and

$$\lambda_2 = \mu_4^2 \sim \frac{A_2}{D_2}. \tag{4.58}$$

The matrix of eigenvectors **Q** becomes, in this approximation,

$$\mathbf{Q} \sim \begin{bmatrix} -1 & -\dfrac{\delta D_2}{D_1} \\ -\dfrac{g_2}{g_1}\dfrac{w}{A_2} & 1 \end{bmatrix}. \tag{4.59}$$

Hence the solutions are found to be

$$n_1(r, v_z) \sim \frac{M_{1,0}\Gamma}{\Delta} + c_3 I_0(\mu_3 r) + c_4 \frac{\delta D_2}{D_1} I_0(\mu_4 r) \tag{4.60}$$

and

$$n_2(r, v_z) \sim \frac{M_{2,0}\Gamma}{\Delta} + \frac{g_2}{g_1}\frac{W}{A_2} c_3 I_0(\mu_3 r) - c_4 I_0(\mu_4 r). \tag{4.61}$$

Boundary conditions are necessary in order to evaluate the four constants c_n. One can derive two of the boundary equations by equating the values of $n_i(R_b, v_z)$ found by use of equations (4.60) and (4.61) to the values given by equations (4.48) and (4.49); the remaining conditions can be obtained by performing a similar exercise with the derivatives $\partial n_i / \partial r$. The inversion of these four equations to obtain c_n is straightforward in principle, but the equations are ill conditioned and it is therefore difficult in practice to invert them with accuracy. The cause of this problem is the extreme values of $I_0(\mu_4 R_b)$ and $K_0(\mu_4 R_b)$. For large arguments (Abramowitz and Stegun 1972),

$$I_n(x) \sim \frac{\exp(x)}{\sqrt{2\pi x}} \tag{4.62}$$

and

$$K_n(x) \sim \exp(-x)\sqrt{\frac{\pi}{2x}}. \tag{4.63}$$

Since the values of $\mu_2 R_b$ and $\mu_4 R_b$ may be expected to be of the order of 100 times larger than $\mu_1 R_b$ and $\mu_3 R_b$, it can be seen that the 2nd and 3rd terms on the right hand side of

equations (4.60) and (4.61) differ by a factor of about 10^{50}. Similar considerations apply to equations (4.48) and (4.49). A better way to proceed is to define new constants d_n such that

$$d_1 = c_1, \tag{4.65}$$

$$d_2 = c_2 \exp(-\mu_2 R_b)\sqrt{\frac{\pi}{2\mu_2 R_b}}, \tag{4.66}$$

$$d_3 = c_3 \tag{4.67}$$

and

$$d_4 = c_4 \frac{\exp(-\mu_4 R_b)}{2\pi\mu_4 R_b}. \tag{4.68}$$

Equations (4.48), (4.49), (4.60) and (4.61) can be expressed in these terms as

$$n_1(r,v_z) \sim \begin{cases} N_{1,0}\Gamma - d_1 K_0(\mu_1 r) - d_2 \dfrac{\delta D_2}{D_1} \exp[\mu_2(R_b - r)]\sqrt{\dfrac{R_b}{r}}, & r > R_b \\ \dfrac{M_{1,0}\Gamma}{\Delta} + d_3 I_0(\mu_3 r) + d_4 \dfrac{\delta D_2}{D_1} \exp[\mu_4(r - R_b)]\sqrt{\dfrac{R_b}{r}}, & r < R_b \end{cases} \tag{4.69}$$

and

$$n_2(r,v_z) \sim \begin{cases} N_{2,0}\Gamma + d_2 \exp[\mu_2(R_b - r)]\sqrt{\dfrac{R_b}{r}}, & r > R_b \\ \dfrac{M_{2,0}\Gamma}{\Delta} + \dfrac{g_2}{g_1}\dfrac{w}{A_2} d_3 I_0(\mu_3 r) - d_4 \exp[\mu_4(r - R_b)]\sqrt{\dfrac{R_b}{r}}, & r < R_b. \end{cases} \tag{4.70}$$

The resulting boundary equations are much better conditioned.

The relationship between the absorption coefficient and the laser intensity can now be derived. Because the experiment measures the decrease in intensity of the whole beam of radiation, it is desirable to calculate the average absorption coefficient. The first step in this derivation is to integrate all the quantities in equation (4.36) across the beam profile and then divide the result by πR_b^2. The resulting equation is

$$\frac{2D_i}{R_b}\left.\frac{\partial n_i}{\partial r}\right|_{r=R_b} + \varepsilon_i\Gamma - \sum_{j=1}^{2} h_{\text{in},ij}\,\bar{n}_j = 0 \tag{4.71}$$

where

$$\overline{n_i} = \frac{2}{R_b^2} \int_0^{R_b} dr\, r\, n_i(v_z, r) \tag{4.72}$$

is the average number density per unit v_z interval of state i within the beam. The spatial derivatives in equation (4.71) are a little awkward to deal with because of the relatively large contribution by the d_2 and d_4 terms in equations (4.69) and (4.70). These terms arise because of the short lifetime of the state 2 atoms. As these emerge from within the beam where their population is maintained at an inflated level, they decay quickly to states 0 and 1. The large outward gradient in the concentration of state 2 at the beam boundary is therefore reflected in the large inward gradient of state 1. These flows of atoms are essentially circular in nature and can be shown to, in effect, cancel each other out. However, their presence complicates the derivation and it is better to dispense with them from the start. This can be done very simply by extending the limit of integration to a radius R_b' which is slightly larger than R_b. Because of the rapidly varying exponential terms in equations (4.69) and (4.70), the d_2 and d_4 contributions to the spatial derivatives in equation (4.71) become negligible, although the other terms are altered by only a very small amount. In this approximation, the average concentrations $\overline{n_1}$ and $\overline{n_2}$ are solutions of the equations

$$\frac{2D_1}{R_b} d_1 \mu_1 K_1(\mu_1 R_b) + \varepsilon_1 \Gamma - \sum_{j=1}^{2} h_{\text{in},1j} \overline{n}_j = 0 \tag{4.73}$$

and

$$\varepsilon_2 \Gamma - \sum_{j=1}^{2} h_{\text{in},2j} \overline{n}_j = 0. \tag{4.74}$$

These equations can be inverted in a similar fashion to the treatment of section 4.2.1, since d_1 can be obtained by the method discussed in the first part of the present sub-section. Examples of the distribution $n_1(r)$ calculated using this method are shown as the solid lines on figure 4.4 on the following page. However, a much neater result is obtained if a further approximation is made. Note firstly that $n_1(r)$ is described to an excellent approximation, for $r > R_b'$, by

$$n_1(r, v_z) = N_{1,0}\Gamma - d_1 K_0(\mu_1 r). \tag{4.75}$$

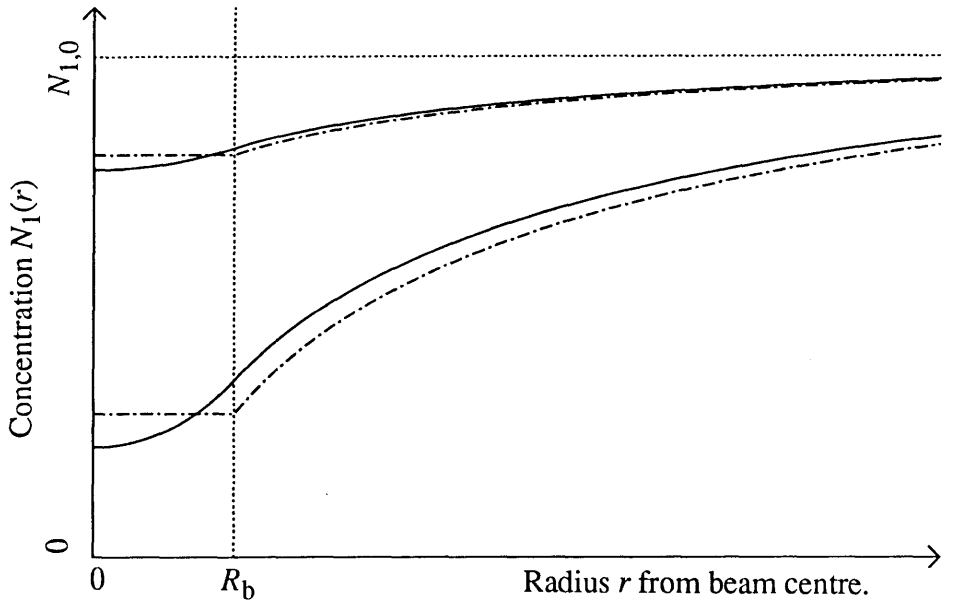

Figure 4.4. The distribution of argon $1s_5$ atoms, at 1 Torr total gas pressure, under the influence of a beam of radiation of radius R_b = 1 mm (this is about 30% larger than the size of beam which was actually used). The laser radiation is tuned to the $1s_5$ - $2p_9$ transition. The concentrations are plotted for two different values of the optical pumping rates w, namely $w/A_{21} = 0.2\%$ and $w/A_{21} = 2\%$. The solid lines represent n_1, the actual concentration per unit interval of the z component of atomic velocity; the chained lines represent the approximation n_1' discussed in the text..

If the value of n_1 which is obtained from this equation at $r = R_b$ is equated to the average value $\overline{n_1}$ within the beam, then the following approximate expression for d_1 may be obtained:

$$d_1 \sim \frac{N_{1,0}\Gamma - \overline{n_1}}{K_0(\mu_1 R_b)}. \tag{4.76}$$

This approximation is equivalent to the replacement of $n_1(r,v_z)$ by

$$n_1'(r,v_z) = \begin{cases} \overline{n_1}, & r < R_b \\ N_{1,0}\Gamma - \dfrac{N_{1,0}\Gamma - \overline{n_1}}{K_0(\mu_1 R_b)} K_0(\mu_1 r), & r > R_b. \end{cases} \tag{4.77}$$

Two examples of the approximation n_1' are compared with n_1 in figure 4.4. Equation (4.73) becomes, in this approximation,

$$\rho_1 N_{1,0}\Gamma + \varepsilon_1\Gamma - \left(\rho_1 + G_1 + \frac{g_2}{g_1}w\right)\bar{n}_1 + (A_{21}+w)\bar{n}_2 = 0, \tag{4.78}$$

where

$$\rho_1 = \frac{2D_1\mu_1 K_1(\mu_1 R_b)}{R_b K_0(\mu_1 R_b)}. \tag{4.79}$$

The inversion of equations (4.74) and (4.78) gives

$$\Delta\bar{n} = \frac{g_2}{g_1}\bar{n}_1 - \bar{n}_2 = \frac{\Delta n_0}{1 + w\Omega_b/A_{21}} \tag{4.80}$$

where

$$\Omega_b = \delta\left(1 + \frac{g_2}{g_1}\frac{A_2}{G_1+\rho_1}\right). \tag{4.81}$$

Clearly, the absorption coefficient in this case is once again given by a relation of the form of equation (4.27), but with I_{sat} now obtained by the substitution of Ω_b for Ω in equation (4.28). Because Ω_b is smaller than Ω, the result in qualitative terms is that, all other things being equal, the onset of saturation is delayed when the radiation is restricted to a thin beam. This makes physical sense, because there is a large reservoir of unperturbed atoms outside the beam, some of which diffuse into the beam, which partially counteracts the depletion by laser radiation of the atoms in state 1.

4.3. Modifications to the free-decay theory.

In this section, a relationship is derived between the average optical pumping rate $\overline{W}$, given by

$$\overline{W} = \frac{\int_{-\infty}^{\infty} dv_z \left[g_2\bar{n}_1(v_z)/g_1 - \bar{n}_2(v_z)\right]w(v_z)}{g_2\overline{N}_1/g_1 - \overline{N}_2}, \tag{4.82}$$

and the rate of free decay of the metastable population after the discharge is extinguished.

The free decay experiment yields useful results only by virtue of the fact that the time dependence of the decay is experimentally observed to be approximated quite well by a single exponential. Models of the process reproduce this feature only if the model

discharge is confined within a cavity. The concentration of metastable particles in the model can then be expanded in a series of spatial eigenmodes of the cavity which decay exponentially at different rates, with the fundamental mode having the longest time constant and therefore soon coming to dominance. An unbounded discharge model such as is described in section 4.2 will not reproduce these features. For this reason, the free decay experiment was analysed in section 3.1.2 in the context of a discharge confined between two infinite parallel planes, which is, in effect, a one-dimensional cavity. When attempting to calculate the change in the rate of free decay of the concentration of metastable particles due to the laser, the spatial non-uniformity of the beam poses problems. The one-dimensional approximation is no longer appropriate. A cylindrical cavity might be used, with the beam of laser radiation crossing the cavity in a direction parallel to its flat faces, but the eigenmodes of such a cavity may be difficult to express in a closed form. For this reason, the analysis in the present section is performed within a model in which the discharge is confined to a cylindrical cavity (of radius R_E) which is traversed by a circular beam (of radius R_b) along the axis of symmetry. This model reproduces (somewhat crudely) the geometry of the actual discharge chamber while remaining reasonably easy to analyse. It is hoped that the qualitative results at least will translate to the actual discharge geometry.

Outside the beam, the number density N_1 obeys the following equation:

$$\frac{\partial N_1}{\partial t} = D_1 \nabla^2 N_1 - G_1 N_1 . \tag{4.83}$$

Here it is assumed that the contribution from the N_2 state falls to a negligible value shortly after the termination of the discharge. (This is a questionable assumption for the region just outside the beam boundary, but this issue is addressed below.) This equation can be solved in a closed cavity by the method of separation of variables, the particular solution being of the form

$$N_1(\mathbf{r},t) = \sum_{n=1}^{\infty} a_n S_n(\mathbf{r}) \exp(-\nu_n t) \tag{4.84}$$

where ν_n is the variable of separation and the functions S_n are eigenfunctions of the spatial equation

$$D_1 \nabla^2 S_n = (G_1 - \nu_n) S_n . \tag{4.85}$$

Formally, equation (4.84) should be expressed as a double sum over separate z- and r-direction indices. (There is no θ dependence because the geometry has full rotational symmetry about the z-axis.) However, because the fundamental eigenmode persists longest in the afterglow and is therefore of most interest for the present discussion, the single index n has, for simplicity, been used to number both types of modes.

In a cavity of cylindrical symmetry, equation (4.85) can be separated again into the following pair of ordinary differential equations:

$$\frac{d^2Z}{dz^2} = -\left(\frac{n\pi}{d}\right)^2 Z \tag{4.86}$$

and

$$\frac{1}{r}\frac{d}{dr}\left(r\frac{dX}{dr}\right) + k_n^2 X = 0 \tag{4.87}$$

where d is the electrode separation and

$$k_n^2 = \frac{\nu_n - G_1}{D_1} - \left(\frac{n\pi}{d}\right)^2. \tag{4.88}$$

The general solution to equation (4.83) is therefore

$$N_1(\mathbf{r},t) = \sum_{n=1}^{\infty} a_n \exp(-\nu_n t)\sin\left(\frac{n\pi z}{d}\right)\left[J_0(k_n r) + b_n Y_0(k_n r)\right] \tag{4.89}$$

where $J_0(x)$ and $Y_0(x)$ are the Bessel functions of order zero. If the gas pressure is such that the factor β in equation (3.5) can be neglected, the concentration $N_1(r,z,t)$ is zero at the physical boundaries of the cavity. The conditions $N_1(r,0,t) = N_1(r,d,t) = 0$ have already been used to reduce the Z_n functions from the general form

$$Z = a\cos(n\pi z/d) + c\sin(n\pi z/d) \tag{4.90}$$

to the pure sine terms in equation (4.89). Two further constraints are needed to evaluate the constants b_n and k_n. One of these is supplied by the radial boundary condition $N_1(R_E, z, t) = 0$, giving

$$b_n = -J_0(k_n R_E)/Y_0(k_n R_E); \tag{4.91}$$

the other must be found at the edge of the beam.

Within the beam of radiation, the concentration of state 2 cannot be neglected, since it is kept at a significant level by optical pumping. The relevant rate equations are

$$\frac{\partial N_1}{\partial t} = D_1 \nabla^2 N_1 - \left(\frac{g_2}{g_1} W + G_1\right) N_1 + (W + A_{21}) N_2 \tag{4.92}$$

and

$$\frac{\partial N_2}{\partial t} = D_2 \nabla^2 N_2 + \frac{g_2}{g_1} W N_1 - (W + A_2) N_2. \tag{4.93}$$

These coupled partial differential equations can be resolved into a set of coupled ordinary DEs if it is assumed that the dependence of N_1 and N_2 upon t and z is the same; in other words, that

$$N_1(r,z,t) = X_1(r) Z(z) T(t) \tag{4.94}$$

and

$$N_2(r,z,t) = X_2(r) Z(z) T(t). \tag{4.95}$$

Substitution of these expressions into equations (4.92) and (4.93) allows these to be separated into

$$\frac{dT}{dt} = -\nu_n T, \tag{4.96}$$

$$\frac{d^2 Z}{dz^2} = -\left(\frac{n\pi}{d}\right)^2 Z \tag{4.97}$$

$$\frac{D_1}{r}\frac{d}{dr}\left(r\frac{dX_1}{dr}\right) - \left(\frac{g_2}{g_1} W - D_1 k_n^2\right) X_1 + (W + A_{21}) X_2 = 0 \tag{4.98}$$

and

$$\frac{D_2}{r}\frac{d}{dr}\left(r\frac{dX_2}{dr}\right) + \frac{g_2}{g_1} W X_1 - \left[W + A_2 - \nu_n + D_2 (n\pi/d)^2\right] X_2 = 0. \tag{4.99}$$

The mean values

$$\overline{X}_i = \frac{2}{R_b^2} \int_0^{R_b} dr\, r\, X_i(r) \tag{4.100}$$

obey the equations

$$\frac{2D_1}{R_b}X_1'(R_b)-\left(\frac{g_2}{g_1}\overline{W}-D_1k_n^2\right)\overline{X}_1+\left(\overline{W}+A_{21}\right)\overline{X}_2=0 \tag{4.101}$$

and

$$\frac{2D_2}{R_b}X_2'(R_b)+\frac{g_2}{g_1}\overline{W}\overline{X}_1-\left[\overline{W}+A_2-\nu_n+D_2(n\pi/d)^2\right]\overline{X}_2=0. \tag{4.102}$$

Once again, the rapid turnover of state 2 atoms in the vicinity of the beam edge can be neglected by the expedient of extending the range of the integration in equation (4.100) a little beyond the beam boundary. This allows us to neglect the spatial derivative in equation (4.102) and also resolves the concern expressed earlier about the validity of equation (4.89) near the beam boundary. In the limit that the mean optical pumping rate $\overline{W}$ is much less than either A_2 or A_{21}, equations (4.101) and (4.102) therefore become

$$\frac{2D_1}{R_b}X_1'(R_b)-\left(\frac{g_2}{g_1}\overline{W}-D_1k_n^2\right)\overline{X}_1+A_{21}\overline{X}_2=0 \tag{4.103}$$

and

$$\frac{g_2}{g_1}\overline{W}\overline{X}_1=A_2\overline{X}_2, \tag{4.104}$$

where X_1' is now clearly identified with the slope of equation (4.89) at $r=R_b$. From these equations, it is easy to deduce the final boundary condition

$$\left.\frac{\partial N_1}{\partial r}\right|_{r=R_b}=\frac{R_b}{2D_1}\left[\frac{g_2}{g_1}\overline{W}(1-\delta)-D_1k_n^2\right]\overline{N}_1. \tag{4.105}$$

In the previous section, an approximate expression for the mean absorption coefficient was derived by equating the value of $n_1(R_b)$ obtained from a formula valid outside the beam to the mean value of n_1 within the beam. In terms of the quantities in the present section, this is equivalent to the assumption that $N_1(R_b)$ as given by equation (4.89) is equal to $\overline{N}_1$. If this approximation is retained, it can be shown by the use of equations (4.89) and (4.91) that k_n is a solution of the transcendental equation

$$\frac{2D_1k_n}{R_b\left[g_2\overline{W}(1-\delta)/g_1-D_1k_n^2\right]}=\frac{J_0(k_nR_b)Y_0(k_nR_E)-J_0(k_nR_E)Y_0(k_nR_b)}{J_0(k_nR_E)Y_1(k_nR_b)-J_1(k_nR_b)Y_0(k_nR_E)}. \tag{4.106}$$

Once k_n has been approximated, the decay constants ν_n can be found by the inversion of equation (4.88).

Limiting values of k_n can be obtained as follows. In the absence of optical pumping, the whole discharge volume is described by equation (4.89); the b_n must therefore equal zero to avoid a singularity at $r = 0$. It is easily seen that $k_{n,\min}$, the minimum value of k_n, must be equal to ζ_n/R_b, where ζ_n is the nth zero of the Bessel function $J_0(x)$. In the opposite limit, $\overline{W} \to \infty$ and therefore $N_1 \to g_1 N_2/g_2$ inside the beam. Since N_2 is always much less than $N_{1,0}$ because of the rapid decay of state 2, a good approximation to this condition is $N_1 \to 0$. In this case the equation in k_n becomes

$$J_0(k_{n,\max}R_b)Y_0(k_{n,\max}R_E) = J_0(k_{n,\max}R_E)Y_0(k_{n,\max}R_b). \tag{4.107}$$

In figure 4.5, $k_1/k_{1,\min}$ is shown as a function of laser intensity I. It can be seen that, whereas the perturbation saturates for quite small values of I, the maximum perturbation is less than 25%.

The mean optical pumping rate $\overline{W}$ is related to the mean absorption coefficient $\overline{k}$ by

$$\overline{W} = \frac{\overline{k} I \lambda_T}{hc\overline{\Delta N}}. \tag{4.108}$$

From equation (4.80), $\overline{\Delta N}$ is given by

$$\overline{\Delta N} = \Delta N_0 \int_{-\infty}^{\infty} \frac{\Gamma(v_z)\,dv_z}{1 + w\Omega_b/A_{21}}. \tag{4.109}$$

This may be re-arranged into the form

$$\overline{\Delta N} = \Delta N_0 \left[1 - a \int_{-\infty}^{\infty} \frac{\Gamma(v_z)\,dv_z}{(v_z - v_{z,0})^2 + a + b} \right] \tag{4.110}$$

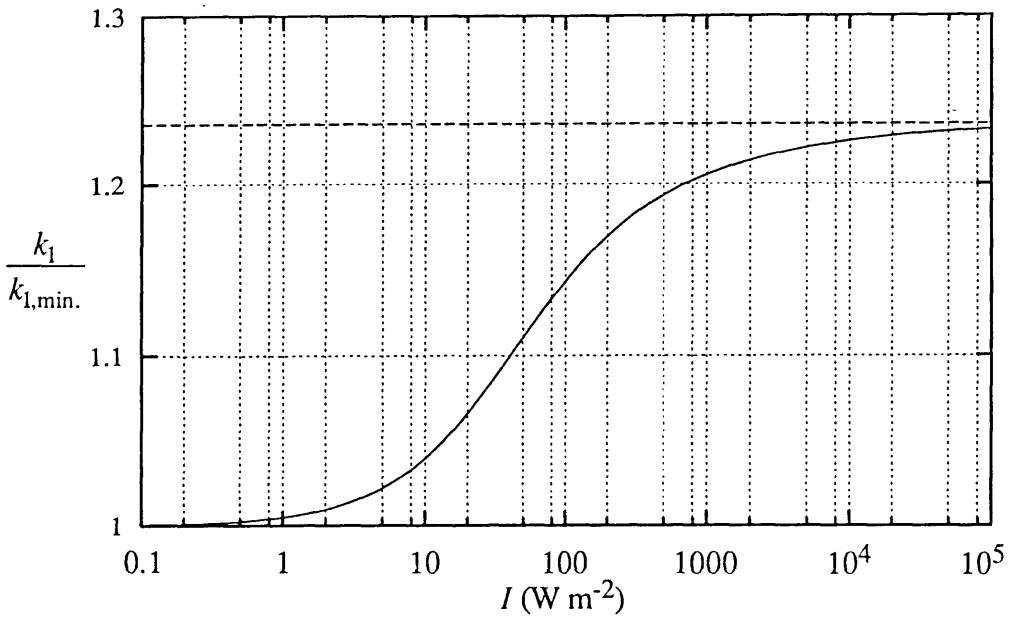

Figure 4.5. The increase in the parameter k with laser intensity. The dashed line indicates the asymptotic value. The transition parameters used to calculate the solid curve are those of the argon $1s_5$ - $2p_9$ transition at pressure of 1 Torr. The beam radius R_b and the electrode radius R_e were taken to be 0.1 cm and 3 cm respectively. A value of 100 s^{-1} was assumed for G_1, the quenching rate of the metastable level; the diffusion coefficients D of both states were assigned the same value of 50 cm^2 s^{-1}. These discharge parameters are also appropriate for argon at 1 Torr.

where

$$a = \frac{\Omega_b I \lambda_T^5 \Delta f_H}{16\pi^2 hc} \tag{4.111}$$

and

$$b = \left(\frac{\lambda_T \Delta f_H}{2}\right)^2. \tag{4.112}$$

Once again the Lorentzian part of the integrand is a much more rapidly varying function than the Gaussian Γ under the present range of experimental conditions; equation (4.110) may therefore be approximated by moving Γ outside the integral sign. The remaining integral is the same one that was discussed in section 4.2.1.1. The solution is therefore

$$\overline{\Delta N} = \Delta N_0 \left[1 - \frac{\Omega_b I \lambda_T^4 \Gamma(v_{z,0})}{\sqrt{1 + I/I_{sat}}}\right] \tag{4.113}$$

where I_{sat} is obtained, once again, by replacing Ω in equation (4.28) by Ω_b. Note that, by use of the appropriate value of Ω, this expression, like that for k, can be used in any of the three absorption situations which have been discussed in section 4.2.

4.4. Conclusion.

The basic purpose of this chapter has been to evaluate the effect of resonant laser radiation upon the discharge and to calculate the relationship between the amount of light absorbed and the number densities of absorbing atoms. Several factors complicate the analysis, including the relatively close spacing of both the 1s and 2p manifolds in argon, the high intensity of the laser radiation and the narrow beam profile.

It was shown in section 4.1.1. that (unlike the case of neon) the collisional interaction between the argon 1s levels is too weak to have a significant effect upon the free decay rates; each 1s state decays at its characteristic rate. However, the 2p levels are much more closely spaced and interactions between these levels must be taken into account when analysing the laser absorption experiment. This is particularly important for those transitions, such as the $1s_5$ - $2p_9$, in which the radiative branching ratio is very close to 1. Collisional mixing of the upper level with other 2p states may then have a large influence upon the onset of saturation.

Saturation of the absorption coefficient occurs when the incident light is intense enough to deplete the population of lower-state atoms by a significant amount. Saturation was investigated in section 4.2 and was shown to be significant at the intensities of irradiation that were used in the present experiments. The reason for this is the inhomogeneous broadening of the argon 1s - 2p transitions at the pressures and temperatures used in the experiment. The narrow-band laser radiation therefore interacts only with those atoms within a small velocity subclass, these atoms being rapidly 'pumped' to the higher level and thus bleaching the transition. Two factors offset this situation by increasing the effective pool of atoms with which the laser radiation is able to interact. The first is the effect of velocity-changing collisions, which ensure there is a constant exchange of atoms between the velocity subclasses. The second factor is the diffusion of fresh 1s atoms into the beam of radiation. A rigorous calculation of the absorption coefficient k as a function of laser intensity I would necessarily include both these effects. Although such a calculation was felt to be beyond the scope of the present study (calculation of the effects

of velocity-changing collisions being particularly intractable), each factor was examined separately and at a relatively unsophisticated level of approximation. The important result of this investigation is that the functional form of the variation of k with I is the same in each case; one might expect, therefore, that the true relation would preserve this form. This was found experimentally to be the case (see figures 10.3 and 10.4 on pages 192 and 193). This result allows the absorption to be predicted at any laser intensity following a preliminary measurement to establish the value of the saturation parameter I_{sat}.

It is desirable to calculate the amount of perturbation by the laser of the rates of free decay of the excited states. Although an exact solution could not be found for the experimental geometry which was used by the author, an approximate analysis was performed. This indicated that the maximum amount of perturbation was unlikely to be large, being of the order of 20 s^{-1} for $1s_5$ states in 1 Torr of argon within a cylindrical discharge chamber of radius 3 cm and electrode separation 1 cm. This is of the order of the contribution from impurities and can be compensated by similar means.

Tables are given on the following pages which list various quantities associated with the argon 1s levels and also with some of the allowed 1s - 2p transitions.

Table 4.1. Characteristics of the argon 1s levels.

	J	E (eV)	Natural lifetime (sec)[a]	'Trapped' life-time τ_t (sec)[c]	F (10^{-32} cm^6 s^{-1})[d]
$1s_2$	1	11.84	2.15×10^{-9}	1.51×10^{-4}	0.2
$1s_3$	0	11.73	44.9[b]	-	1.0
$1s_4$	1	11.63	8.6×10^{-9}	1.49×10^{-4}	1.2
$1s_5$	2	11.56	55.9[b]	-	1.2

Notes:

a: From Lawrence (1968), except where otherwise indicated.

b: From Small-Warren and Lue-Yung (1975).

c: Calculated at a pressure of 1 Torr, a temperature of 300K and an electrode separation of 1 cm by use of equation (4.2).

d: These are rough averages of results compiled by Millet *et al* (1981).

Table 4.2. The ratios C_{ji}/C_{ij} (calculated by use of equation (4.4)).

		State j		
		$1s_3$	$1s_4$	$1s_5$
State i	$1s_2$	4.50×10^{-2}	3.04×10^{-4}	2.50×10^{-5}
	$1s_3$		8.80×10^{-3}	2.74×10^{-4}
	$1s_4$			3.24×10^{-2}
	$1s_5$			

Table 4.3. Rates of destruction of the argon 1s levels at 1 Torr, 300 K. Units are s^{-1}.

		$C_{ij}N_0$[a]						
		State *j*						
		$1s_2$	$1s_3$	$1s_4$	$1s_5$	$F_iN_0^2$[b]	$1/\tau_t$[b]	Total
State *i*	$1s_2$		< 3700	?	?	2	6700	~ 10^4?
	$1s_3$	< 167		< 167	< 167	10	-	< 177
	$1s_4$	?	< 1.47		990	12	6700	~ 7700
	$1s_5$	?	< .046	32		12	-	44

Notes:

a: Taken from Ellis and Twiddy (1969). Note, however, that these first-order rates are much larger at pressures over 100 Torr (Manzanares and Firestone 1983).

b: From table 4.1.

Table 4.4. Some characteristics of selected 1s - 2p transitions in argon.

Transition:	λ (nm)	A_{21} (10^6 s^{-1})[a]	δ[b]	γ	2η (MHz)[c]	σ (10^{-15} m^2)	I_{sat} (W m^{-2})
$1s_5$ - $2p_9$	811.531	33.1	0.988	7/5	14	1.124	8.7×10^{-3}
$1s_4$ - $2p_5$	751.465	40.2	0.982	1/3	27	1.084	6.3
$1s_4$ - $2p_7$	810.369	25.0	0.715	1	27	0.845	0.13
$1s_3$ - $2p_2$	772.421	11.7	0.332	3	15	0.343	9.1×10^{-4}
$1s_2$ - $2p_1$	750.384	44.5	0.995	1/3	109	1.194	63

Notes:

a: Taken from Wiese *et al* (1989).

b: The total decay rate used in the calculation of the branching ratios includes the effects of collisional redistribution among 2p states. Rates of collisional distribution were calculated from the data of Nguyen and Sadeghi (1978) using a pressure of 1 Torr.

c: Calculated at 1 Torr and 300 K. Values of $2\eta/N_0$ were taken from Tachibana *et al* (1982), except for the $1s_2$ value, for which was calculated from the data of Vallee *et al* (1976). These widths should be taken to include the contribution due to 'weak' velocity-changing collisions.

5. Theoretical background to optical measurements of electron transport properties in a discharge with a non-point source of current.

In very pure argon, a significant proportion of the total ionisation is due to the production of secondary electrons at the cathode by atoms in the metastable $1s_3$ and $1s_5$ states (Engstrom and Huxford 1940, Molnar 1951b). Two ways of viewing this contribution were examined in chapter 3. On the one hand, the presence of metastable atoms can be considered as something of a nuisance which interferes with measurements of the primary and secondary ionisation coefficients α_i and γ_i; however, because they themselves make an important contribution to the discharge process, metastables are also worthy of study in their own right. In the present chapter, a third aspect is discussed: the possibility of using metastable excited states as a means to assay the number density and average energy of the electrons in the discharge. The rate of increase in the concentration of excited states at the commencement of the discharge can be shown to be approximately proportional to the local density of electric current in the discharge (see section 5.5 below). Measurement of the variation of this rate throughout the discharge can therefore be used as a way of determining some of the electron transport parameters. Because the generation rate is also a function of the mean energy of the electrons, the possibility also exists of using measurements of the rate to probe the extent of the electron non-equilibrium region.

Electron transport parameters have been successfully determined by measuring the light emitted by excited atoms or molecules in a pre-breakdown discharge (Blevin and Fletcher 1992). Although it is, no doubt, possible to apply this method to the argon discharge, it was decided to attempt the direct measurement of number densities of excited particles by means of optical absorption. The two methods have complementary advantages and disadvantages. Detection of light emission involves the direct measurement of a signal against a minimal background, and does not itself perturb the discharge; on the other hand, it is easier to obtain spatial resolution and state specificity within the context of an absorption experiment. Also, it is easier to determine absolute values of the concentrations of excited states, which are necessary to determine the state excitation coefficient α_m, by measuring the amount of light the atoms absorb.

In order to analyse either absorption or emission measurements, it is necessary to know the relationship between the distribution of electrons and the electron transport parameters. Previous authors (eg Lucas 1964 and 1965, Huxley 1972) calculated number

density profiles of electrons in a variety of situations; for various reasons, none of these treatments is applicable to the present experiment. The purpose of this chapter is to provide this required theoretical background.

The theory given below represents a compromise between two conflicting aims: to make the theory as complete as possible while retaining a degree of mathematical simplicity. Many approximations have been made, for example, in the treatment of the secondary current. This approach is justified in the final section, where it is shown that useful information about the transport parameters can be gained from an analysis that is independent of the distribution and size of the cathode current.

5.1. Properties of the Hankel transform.

The Hankel transform is used in this chapter to solve the electron continuity equation. This transform is defined by

$$\mathscr{H}[f(r):r\to\eta]=\int_0^\infty f(r)J_0(\eta r)r\,dr \tag{5.1}$$

where $J_n(x)$ is the Bessel function of order n. This transform is used because it possesses the following advantages peculiar to the present experiment. Firstly, note that the total amount κ of light absorbed from a thin beam which is parallel to the x axis (see figure 3.1 on page 23 for the geometry) is related to the absorption coefficient k by

$$\kappa(y,z)=\int dx\,k(x,y,z). \tag{5.2}$$

If the concentration of excited states has cylindrical symmetry, k will be a function of r and z alone. The total absorption κ can, in this case, be shown to be given by the Abel transform of $k(r,z)$ (Bracewell 1965):

$$\kappa(y,z)=\mathscr{A}[k(r,z):r\to y]$$

$$=2\int_y^\infty \frac{dr\,r\,k(r,z)}{\sqrt{r^2-y^2}}. \tag{5.3}$$

However, the Hankel and Abel transforms are related as follows (Sneddon 1972):

$$\mathscr{H}[f(r):r\to\eta]=\mathscr{F}_c\{\mathscr{A}[f(r):r\to x]:x\to\eta\} \tag{5.4}$$

where $\mathscr{F}_c$ is the Fourier cosine transform. There are two ways in which experimental results may be compared with theoretical expressions found by using the Hankel transform. The Hankel-transformed solutions may be compared directly with experiment by first performing a Fourier cosine inversion on these solutions; Alternatively, the experimental values can be Fourier transformed (after interpolation if necessary) then compared directly with theory. The use of the Hankel transform therefore allows one to use the Fourier transform rather than an Abel inversion in the reduction of experimental data. This is desirable on computational grounds.

Another advantage of the Hankel transform arises as follows. The number density of electrons in the discharge can be described by the double convolution

$$n(x,y,z)=\int dy'\int dx'\,n(x',y',0)p(x-x',y-y',z) \tag{5.5}$$

where n is here (and in the rest of the chapter) the number density of electrons and p is the point spread function. Because the point spread function carries all the information about the electron transport parameters, it would be desirable to be able to deconvolve this function from the cathode current, which may not be well determined. The Hankel transform allows this to be done as follows. Note firstly that both n and p possess cylindrical symmetry, and can therefore be expressed purely in terms of radial and axial coordinates. In these terms, equation (5.5) becomes

$$n(x,y,z)=\int dy'\int dx'\,n(r',0)p(r'',z), \tag{5.6}$$

where $r'^2=x'^2+y'^2$ and $r''^2=(x-x')^2+(y-y')^2$. The absorption experiment returns information about the number density integrated in the x direction, which is given by

$$N(y,z)=\int dy'\int dx'\,n(r',0)\int dx\,p(r'',z). \tag{5.7}$$

This is equivalent to the single convolution

$$N(y,z) = \int dy' \, \mathscr{A}[n(r',z):r' \to y]\mathscr{A}[p(r'',z):r'' \to y - y']. \tag{5.8}$$

Application of the Fourier cosine transform to both sides gives

$$\mathscr{F}_c[N(y,z):y \to \eta] = \mathscr{H}[n(r',z):r' \to \eta]\mathscr{H}[p(r'',z):r'' \to \eta], \tag{5.9}$$

where equation (5.4) has also been used. A technique of data reduction that makes use of this property is described in section 5.5 below.

5.2. Discharge geometry and processes.

The geometry of the discharge volume, depicted in figure 3.1, page 23, is the same as that used to model the free decay of the concentration of metastables in chapter 3. In the centre of one of the electrodes is a circular quartz window, of radius R_w, which is coated with a semi-transparent layer of gold. The primary cathode current is generated photoelectrically by an external source of ultraviolet light. This light passes through the window, about half being absorbed by the gold film, the rest impinging upon the opposite electrode. Either electrode can therefore be used as the cathode, depending on the polarity of the potential difference between the electrodes. The masking effect of the window ensures that the primary current $j_{prim}(r)$ from either electrode is given to a good approximation by the step-function form

$$j_{prim}(r) = \begin{cases} j_{prim}, & r < R_w \\ 0, & r > R_w. \end{cases} \tag{5.10}$$

Additional electrons are generated in the discharge by collision between drifting electrons and gas atoms at a rate equal to $w\alpha_i n$, where **w** is the electron drift velocity and α_i is Townsend's primary ionization coefficient. Secondary electrons may also be ejected from the cathode by the incidence of ions, excited atoms or resonant photons; however, as discussed in chapter 2 section 2.2, the contribution made by excited states or photons can be either subtracted or neglected.

5.3. The electron diffusion equation; boundary conditions.

The Boltzmann equation for the density of electron states can be approximated in the hydrodynamic regime by a second order continuity equation in the electron density $n(\mathbf{r})$ (eg Skullerud 1974, Kumar *et al* 1980):

$$\mathbf{D}:\nabla\nabla n - \mathbf{w}\cdot\nabla n + w\alpha_i n = \frac{\partial n}{\partial t} \tag{5.11}$$

where **D** is the electron diffusion tensor. If the discharge has cylindrical symmetry, the steady state form of equation (5.11) can be expressed in cylindrical polar coordinates as

$$D\left(\frac{\partial^2 n}{\partial r^2} + \frac{1}{r}\frac{\partial n}{\partial r}\right) + D_L\frac{\partial^2 n}{\partial z^2} - w\frac{\partial n}{\partial z} + w\alpha_i n = 0 \tag{5.12}$$

where the notation $D = D_{xx} = D_{yy}$ and $D_L = D_{zz}$ has been used to conform with previous work, and the off-diagonal elements of **D** are assumed to be zero (Huxley & Crompton 1974). The radial diffusion coefficient D has been distinguished from D_L as it has been well established that they are unequal (eg Wagner *et al* 1967).

Lowke *et al.* (1977) and Skullerud (1974) showed that the continuity equation becomes a poor approximation to the motion of the electron swarm within boundary layers which extend for a distance of about D/w from the electrodes. It might therefore seem that equation (5.12) is unusable under any circumstances because sensible boundary conditions cannot be imposed. However, it has been found that solutions of equation (5.12) conform closely in shape to experimentally determined electron distributions away from the electrode boundary layers (see e.g. Blevin *et al.* 1976a, 1976b, 1978). It therefore seems likely that the main effect of these layers is to make it impossible to use equation (5.12) to determine with accuracy the amplitude of the number density function. The emphasis in this chapter has therefore been placed upon the determination of transport parameters by the use of ratios in, rather than absolute values of, the electron number density.

The next problem to address is the selection of physically reasonable boundary conditions. The author will follow the practice of previous authors (Huxley 1972, Lucas 1965) in adopting, at the anode, the boundary condition $n(d) = 0$ (where d is the electrode

separation). Whereas the anode might be expected to exert a purely local perturbation upon the electron distribution, the effect of the cathode is more fundamental. This is because the streaming of electrons from cathode to anode ensures that a large fraction of the electrons making up the bulk of the discharge have come straight from the cathode. The electron distribution throughout the entire discharge volume thus depends crucially on the distribution of current leaving the cathode. These electrons are ejected from the cathode surface with a highly non-thermal velocity distribution, their average energy being generally lower than the equilibrium value (Haydon and Williams 1973b). The lower energy of the electrons in the cathode layer results in a variation in the ionization rate α_i within this layer. A method of accounting for this variation is examined in section 5.4.2.

Another problem at the cathode is that the current at a small distance from this electrode is less than the current of electrons actually ejected from its surface. This is because some of the ejected electrons are immediately reflected by gas molecules back into the surface. Now, the total current density $\mathbf{j}(r,z)$ in the equilibrium region far from the electrodes is

$$\mathbf{j}(r,z) = e\left[\mathbf{w}\, n(r,z) - \mathbf{D}\nabla n\right] \tag{5.13}$$

where e is the electronic charge; the z component of the current density is therefore given by

$$j_z(r,z) = e\left[w\, n(r,z) - D_{\mathrm{L}} \frac{\partial n}{\partial z}\right]. \tag{5.14}$$

(Here it has been assumed that $w_z = w$.) It is tempting to identify the backscattered electrons with the diffusive part of j_z in equation (5.14), and therefore to equate the ejected current density to the drift current density $e\,w\,n(r,0)$. This was essentially the approach adopted by Huxley (1972), who used a dipole source of electrons at the centre of the cathode. This type of source ensured that $n(r,0) = 0$ for $r > 0$, which agrees with the commonly accepted idea that n becomes zero at an absorbing surface. This approach cannot be used if the current source is extended across the cathode, however, because there may then be places on the cathode where $\partial n/\partial z|_{z=0}$ is negative; equation (5.14) then gives a value of $j_z(r,0)$ which is *larger* than the ejected current density. To avoid this impossibility, the cathode boundary condition adopted throughout the present work is obtained by equating the value of $j_z(r,0)$ given by equation (5.14) to some constant fraction of the flux of electrons ejected from the cathode. In other words, let

$$j_z(r,0) = q\left[j_{\text{prim}}(r) + e\gamma_i\phi_i(r,0) + e\gamma_m\phi_m(r,0)\right] \qquad (5.15)$$

where q is the constant of proportionality, $j_{\text{prim}}(r)$ is the density of the primary current and the symbols γ and $\phi(r,0)$ represent, respectively, the electron ejection efficiency and flux into the cathode of ions (subscript 'i') and metastable atoms (subscript 'm'). However, in the present chapter, attention is directed at fast processes rather than those arising from the diffusion of metastable particles. As is shown in section 5.5, the concentration of metastable atoms is proportional to that of the electrons only within a timescale which is too short for significant diffusion of neutral particles to occur. The contribution made by metastable-ejected secondary electrons to the total current is therefore neglected in the ensuing analysis.

The Hankel transform can only be applied to equation (5.12) if the discharge space is unbounded in the radial direction. The results of the present chapter are therefore only applicable to a real discharge between parallel planar electrodes if the concentration of electrons falls to an insignificant value at the boundary of the electrodes. The conditions under which this occurs are discussed further in chapter 6.

5.4. A new method of solving the diffusion equation with an extended source of current.

5.4.1. General solution.

For discharge regimes where the electron number density at the electrode edges is negligible, the discharge may be modelled by a space bounded by infinite plane electrodes, but with the primary current restricted to a circularly symmetrical region concentric with the origin of coordinates. Solutions using this model have been found for a point source of primary current (Huxley 1972), but none have been proposed for an extended current source. Such a solution is developed in this section.

In the above geometry, the zero-order Hankel transform defined by equation (5.1) can be used to solve equation (5.12). Although it is generally difficult to back-transform the solutions analytically to obtain closed-form expressions for $n(r,z)$, this can be done numerically if desired.

The transformed steady-state electron distribution $N(\eta,z)=\mathscr{H}[n(r,z):r\rightarrow\eta]$ obeys the differential equation

$$\frac{\partial^2 N}{\partial z^2}-2\lambda\frac{\partial N}{\partial z}+\left[\lambda^2-u^2(\eta)\right]N=0 \tag{5.16}$$

where

$$\lambda=w/2D_L \tag{5.17}$$

and

$$u^2(\eta)=\lambda^2-2\lambda\alpha_i+\eta^2 D/D_L\,. \tag{5.18}$$

There are two possibilities: either $u^2(0)>0$ or $u^2(0)\leq 0$. The first case only will be considered here, since $\lambda >> 2\alpha_i$ in most discharge regimes of interest. In this case the general solution to equation (5.16) is

$$N(\eta,z)=A(\eta)\exp\left[(\lambda-u)z\right]+B(\eta)\exp\left[(\lambda+u)z\right]. \tag{5.19}$$

Application of the electrode boundary conditions described in Section 5.3 gives the particular solution

$$N(\eta,z)=\frac{\zeta(\eta,0)}{eD_L\beta(\eta)}\left\{\exp\left[(\lambda-u)z\right]-\exp\left[(\lambda+u)z-2ud\right]\right\} \tag{5.20}$$

where

$$\zeta(\eta,0)=\mathscr{H}[j_z(r,0):r\rightarrow\eta] \tag{5.21}$$

and

$$\beta(\eta)=\lambda+u-(\lambda-u)\exp(-2ud). \tag{5.22}$$

The electron distribution can be found by back-transforming, ie

$$n(r,z)=\int_0^\infty N(\eta,z)J_0(\eta r)\,\eta\,d\eta. \tag{5.23}$$

In the pre-breakdown regime, most of the cathode current $j_z(r,0)$ will be concentrated within the window area of radius R_w. This is because the current within this area arises from both primary and secondary contributions, whereas the current density at greater radius is due only to secondary sources. The function $j_z(r,0)$ may therefore be

expected to have a shape that is peaked at $r = 0$, decreasing asymptotically to zero as $r \rightarrow \infty$. The width of this function at half maximum will be of the order of R_w. Recall that the space-bandwidth product, found by multiplying the respective half-maximum widths of a function and its Fourier transform, is approximately equal to 2π. Because the Hankel-transformed cathode current $\zeta(\eta, 0)$ represents a radial 'slice' through the two-dimensional Fourier transform of $j_z(r,0)$ (Sneddon 1972), one might therefore expect the amplitude of $\zeta(\eta, 0)$ to be negligible at values of η much greater than $2\pi/R_w$. A good approximation to the solution $n(r,z)$ may therefore be obtained by truncating the integral in equation (5.23) at some value $\eta' > 2\pi/R_w$. Equation (5.23) could then be integrated numerically using a discrete Hankel transform.

An example of a solution is shown in figure 5.1, on the following page.

It is possible to further manipulate equation (5.20) so that it is only necessary to have *a priori* knowledge of the distribution of primary current. The first step in this procedure is to consider the flux of ions onto the cathode. This is easy to calculate if the radial diffusion of the ions can be neglected. Consider a cloud of ions originating at a point source on the anode. The radial spread of this cloud may be estimated by calculating the mean radial displacement $|\bar{r}|$ of the ions. McDaniel (1964b) gives, as the ratio between $|\bar{r}|$ and the electrode separation d,

$$\frac{|\bar{r}|}{d} = \frac{0.172}{\sqrt{V}} \tag{5.25}$$

where V is the potential difference between the electrodes. Clearly the sideways diffusion of ions can be neglected for values of V larger than about 5 volts. Hence we may write

$$\Phi_i(\eta, 0) = w\alpha_i \int_0^d N(\eta, z)\, dz \tag{5.26}$$

$$= \frac{2\lambda\alpha_i\zeta(\eta,0)}{e(\lambda^2 - u^2)} \left\{ \frac{2u}{\beta} \exp[(\lambda - u)d] - 1 \right\}. \tag{5.27}$$

where Φ_i is here the transformed cathodic ion flux density. Equation (5.27), when inserted into the Hankel transform of equation (5.15), allows the reformulation of equation (5.20) as

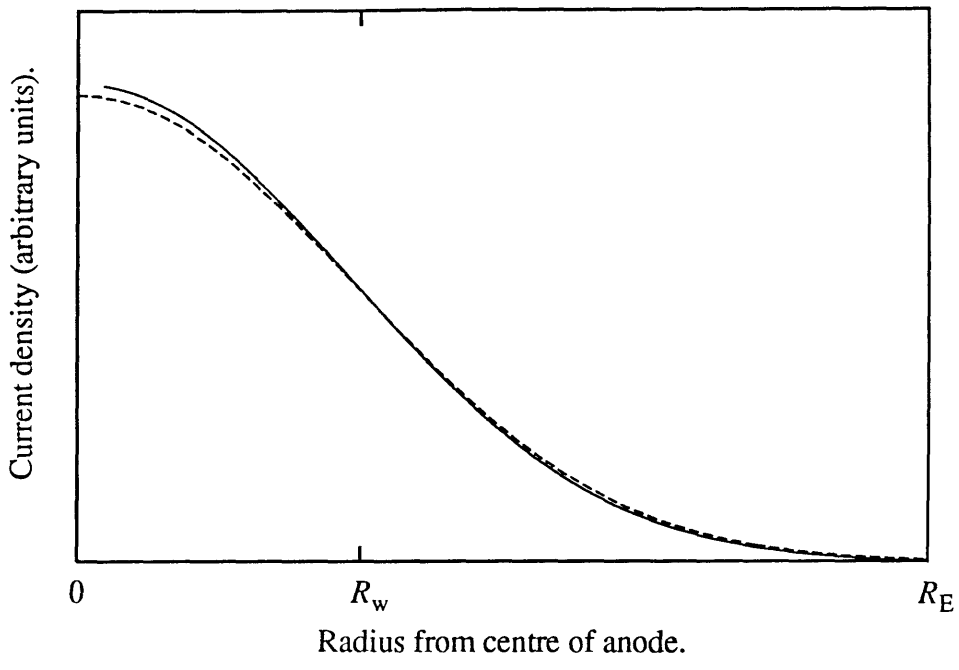

Figure 5.1. A comparison between exact (solid line) and approximate (dashed line) distributions of current at the anode. The exact solution was obtained by a numerical Hankel inversion of equation (5.20), using the algorithm of Siegman (1977); the gap in the curve near the *y* axis is an artifact of this algorithm. The approximate solution is that given by equation (5.51). (In both cases, electron concentrations were converted to current densities by the use of equation (5.14).) For the sake of the example, secondary processes were neglected and the primary current was taken to have the step-function form given in equation (5.10). The transport parameters used are similar to those measured by Townsend and Bailey (1922), Kruithof (1940) and Nakamura and Kurachi (1988) for a discharge in argon at a reduced electric field *E/N* of 20 Td. (1 Td equals 10^{-17} V cm^2.) An electrode separation of 2.5 cm and a pressure of 10 Torr were assumed. The values used for R_w and R_E were, respectively, 1 and 3 cm.

$$N(\eta,z)=\frac{qS(\eta)\zeta_{\text{prim}}(\eta,0)}{eD_L\beta}\left\{\exp\left[(\lambda-u)z\right]-\exp\left[(\lambda+u)z-2ud\right]\right\} \tag{5.28}$$

where

$$\zeta_{\text{prim}}(\eta,0)=\mathscr{H}\left[j_{\text{prim}}(r):r\rightarrow\eta\right] \tag{5.29}$$

and

$$\frac{1}{S(\eta)}=\left\{1-\frac{2q\lambda\alpha_i\gamma_i}{\lambda^2-u^2}\left[\frac{2u}{\beta}\exp[(\lambda-u)d]-1\right]\right\}. \tag{5.30}$$

If $u(\eta)=\lambda$ for any η, $S(\eta)$ becomes, for that value of η,

$$\frac{1}{S(\eta)} = \left\{1 - \frac{q\alpha_i\gamma_i}{2\lambda}\left[(2\lambda d + 1)\exp(-2\lambda d) - 1\right]\right\}. \tag{5.31}$$

In the case that the primary current is generated by the backlighting of a circular window, as described in section 5.2, $j_{prim}(r)$ will have the form given in equation (5.10). The Hankel transform of this function is

$$\zeta_{prim}(\eta, 0) = j_{prim} R_w J_1(\eta R_w)/\eta. \tag{5.32}$$

Note that S as given by equation (5.30) is singular if

$$\frac{2q\lambda\alpha_i\gamma_i}{\lambda^2 - u^2}\left\{\frac{2u}{\beta}\exp\left[(\lambda - u)d\right] - 1\right\} = 1. \tag{5.33}$$

S can be shown to be non-singular for all η at electrode separations d less than some value d_{bd}; at this separation, the singularity occurs at $\eta = 0$. No solution exists at this separation because the inverse transform in equation (5.23) does not converge in this case. This singularity corresponds to the electrical breakdown of the gas.

5.4.2. Effects of the variation of α_i near the cathode.

As mentioned in section 5.3 above, the effective ionization coefficient may vary in the cathode non-equilibrium layer. An analytical solution is possible if the step-function approximation given in equation (2.4) is used, albeit at the expense of greater mathematical complexity. The solution N then becomes

$$N(\eta, z) = A(\eta) \times \begin{cases} B(\eta)\exp\left[(\lambda - u')z\right] + C(\eta)\exp\left[(\lambda + u')z\right], & z < d_0 \\ \exp\left[(\lambda - u)z\right] - \exp\left[(\lambda + u)z - 2ud\right], & z > d_0 \end{cases} \tag{5.34}$$

where

$$(u')^2 = \lambda^2 + \eta^2 D/D_L. \tag{5.35}$$

The coefficients A, B and C can be evaluated by appropriate use of the boundary conditions at $z = 0$, d_0 and d. When secondary current is included, an expression with the same general form as equation (5.28) is obtained. The parameter S' that has the same role as the S in equation (5.28) is given by

$$S'(\eta) = \left[1 - \frac{2q\lambda\alpha_i\gamma_i}{\beta'(\eta)} W(\eta)\right]^{-1} \tag{5.36}$$

where

$$\beta'(\eta) = B(\eta)(\lambda + u') + C(\eta)(\lambda - u') \tag{5.37}$$

and

$$W(\eta) = 2u\exp[(\lambda - u)d] - \{(\lambda + u) - (\lambda - u)\exp[-2u(d - d_0)]\}\exp[(\lambda - u)d_0]. \tag{5.38}$$

In figure 5.2, three distributions of anode current are plotted. The transport parameters used here are similar to those measured by Blevin *et al* (1976b and 1978) for a discharge in hydrogen at 200 Td and 0.5 Torr. Hydrogen is used instead of argon in this example because the cathode non-equilibrium layer is relatively large in hydrogen. Folkard and Haydon (1971a, b) measured the true thickness d_0' and the effective thickness d_0 of this layer to be about 1.6 cm and 0.6 cm respectively at the above values of electric field and pressure. An electrode separation of 2.5 cm has been used in the present example, the secondary ionization coefficient γ_i being arbitrarily set to one half of the value required to produce electrical breakdown of the gas at this distance. Values of 1 and 3 cm were used for R_w and R_E.

The solid line in figure 5.2 represents the distribution of anode current calculated by using the step-function approximation for α_i, with d_0 given its correct value of 0.6 cm. The dotted line is the solution obtained using the cruder approximation that $d_0 = 0$. The two curves have been normalised to the same total anode current, but are clearly different in shape. However, most of this difference arises from the spread of the discharge across the cathode as the proportion of secondary to primary current increases in the approach to breakdown. In fact the error in the shape of the $d_0 = 0$ solution can be largely corrected by using an effective value of γ_i scaled so that the ratio between the total primary cathode current and the total secondary cathode current is the same for the two cases. This can be achieved by setting $S(0)$ equal to $S'(0)$. A fair approximation to this condition can be

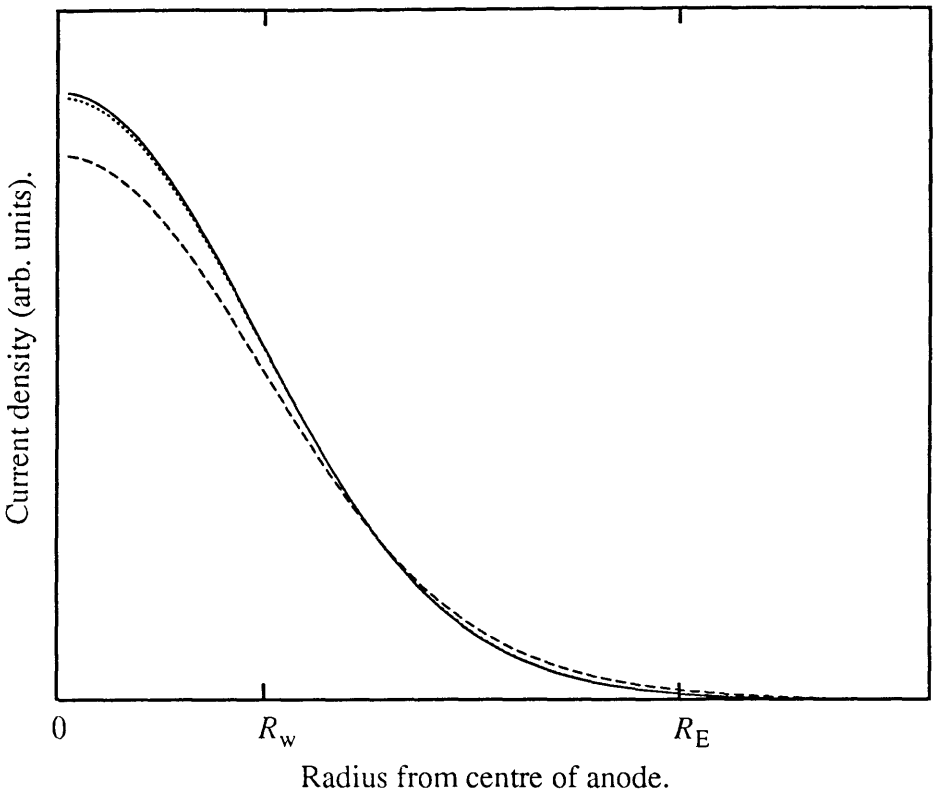

Figure 5.2. A comparison between various models of the anode current distribution in a hydrogen discharge at 200 Td and 0.5 Torr. The solid line was calculated by assuming that d_0 in equation (2.4) is equal to 0.6 cm; the dashed line is the result obtained by use of the simpler but cruder approximation $d_0 = 0$. This approximation was retained when calculating the dotted curve, but an effective value of the secondary coefficient was obtained by using equation (5.39). All curves were normalised to the same total anode current.

obtained by neglecting the influence of longitudinal diffusion, giving a value for the effective coefficient γ_i' of

$$\gamma_i' = \gamma_i \frac{\exp(\alpha_i d - \alpha_i d_0) - 1}{\exp(\alpha_i d) - 1}. \tag{5.39}$$

A third solution was calculated, using the (simpler) $d_0 = 0$ analysis, but with an effective γ_i' calculated using equation (5.39). When the resulting current density is plotted, normalised again to the same value of total anode current as the solution with $d_0 = 0.6$ cm, these two curves vary by less than 1%.

Note that the parameters necessary to apply equation (5.39) can be independently calculated by measurements of the total current passed by the discharge at varying d (see, for example, Haydon and Williams 1976).

5.4.3. Approximate solutions.

Equation (5.18) can be rewritten as

$$u^2(\eta) = u_0^2\left(1+\frac{\eta^2 D}{u_0^2 D_L}\right) \tag{5.40}$$

where the shorthand $u_0 = u(0)$ has been used. Expanding $u(\eta)$ in terms of η gives

$$u(\eta) = u_0 + \frac{\eta^2 D}{2u_0 D_L} + O(\eta^4). \tag{5.41}$$

This series converges provided that

$$\eta < u_0\sqrt{\frac{D_L}{D}}. \tag{5.42}$$

The transformed number density N given by equation (5.20) may therefore be approximated at small values of η by

$$N(\eta, z) \sim \frac{\zeta(\eta,0)}{eD_L\beta_0} Z_0(z)\exp\left(-\frac{\eta^2 Dz}{2u_0 D_L}\right) \tag{5.43}$$

where

$$Z_0(z) = \exp[(\lambda - u_0)z] - \exp[(\lambda + u_0)z - 2u_0 d]. \tag{5.44}$$

In section 5.4.1 it was shown that N becomes negligible at values of η greater than $2\pi/R_w$. Equation (5.43) can, therefore, be used in place of equation (5.20), provided that

$$\frac{2\pi}{R_w} < u_0\sqrt{\frac{D_L}{D}}. \tag{5.45}$$

Use of the assumption made in section 5.4.1 that $\lambda >> 2\alpha_i$ changes this condition to

$$wR_w > 4\pi\sqrt{DD_L}\,. \tag{5.46}$$

This condition is satisfied by many monatomic and diatomic gases at values of R_w of around 1 cm, if the pressure is greater than about 1 Torr.

The solution of equation (5.43) is obtained formally by a reverse transform:

$$n(r,z) \sim \frac{Z_0(z)}{eD_L\beta_0}\int_0^\infty \zeta(\eta,0)\exp\left(-\frac{\eta^2 Dz}{2u_0 D_L}\right)J_0(\eta r)\,\eta\,d\eta. \tag{5.47}$$

In the small signal limit, $j_z(r,0)$ has the step function form described by equations (5.10) and (5.24). The Hankel transform of this current distribution is given in equation (5.32). If $\zeta(\eta,0)$ has this form, the right hand side of equation (5.47) can be expressed in terms of a tabulated function. The insertion of equation (5.32) into equation (5.47) and the use of the replacements

$$x^2 = \frac{u_0 D_L}{2zD}R_w^2, \tag{5.48}$$

$$y^2(r) = \frac{u_0 D_L}{2zD}r^2 \tag{5.49}$$

and

$$t^2 = \frac{zD}{2u_0 D_L}\eta^2 \tag{5.50}$$

produces

$$n(r,z) \sim \frac{qj_{prim}Z_0(z)}{eD_L\beta_0}\left[2x\int_0^\infty \exp\left(-t^2\right)J_0[2y(r)t]J_1(2xt)\,dt\right]. \tag{5.51}$$

The term in square brackets is the function $x^2\sqrt{\pi}\,F(x,y)$ described by Luke (1962b) and references therein. It is tabulated as $P\left(x\sqrt{2},y\sqrt{2}\right)$ in Masters (1955).

A plot of the anode current obtained using equation (5.51) is compared in figure 5.1 with the exact solution derived in section 5.4.1. The same transport parameters (ie, argon at 20 Td, 10 Torr) were used. Even though the inequality (5.46) is only marginally obeyed under these circumstances, the two curves can be seen to agree well, indicating that the approximation given in equation (5.47) is a valid one.

5.5. New techniques of data reduction.

The experiment uses a 'chopped' ultraviolet light source to generate bursts of primary current. As mentioned in the introduction to this chapter, changes in the number density of excited states were monitored by measuring the optical absorption integrated along a path through the discharge. The number density n_j of the jth excited state obeys a diffusion equation of the form (see chapter 2.2.2)

$$\frac{\partial n_j}{\partial t} = w\alpha_j(\mathbf{r},t)n(\mathbf{r}) + D_j\nabla^2 n_j - \frac{n_j}{\tau_j} \tag{5.52}$$

where α_j is the total rate of electronic excitation, D_j is the diffusion coefficient and τ_j the lifetime of the state. The time dependence of the excitation rate arises from cascaded contributions from states of higher energy (Fletcher and Reid 1980). Provided that the maximum lifetime τ of these states is significantly shorter than τ_j, an intermediate time scale $\tau < t < \tau_j$ can be defined in which the rate of increase of n_j is given approximately by

$$\frac{\partial n_j}{\partial t} \sim w\alpha_j(\mathbf{r})n(\mathbf{r}). \tag{5.53}$$

Within this intermediate time scale, the rate of rise $\dot{\kappa}(x,z)$ of the total optical absorption along a line parallel to the y axis will therefore be given by

$$\dot{\kappa}(x,z) = \frac{1}{I}\frac{dI}{dt} = w\sigma\int_{-\infty}^{\infty}\alpha_j(\mathbf{r})n(\mathbf{r})\,dy \tag{5.54}$$

where σ is the absorption cross-section. In deriving this expression it has been assumed that the absorber is optically thin and that the light is monochromatic and tuned to a transition of the jth excited state. The value of α_j depends on the mean energy of the electrons. The conditions under which this is approximately spatially invariant have been discussed in section 5.3. Where this invariance holds, it follows that

$$\dot{\kappa}(x,z) \propto \int_{-\infty}^{\infty} n(\mathbf{r})\,dy. \tag{5.55}$$

From the identity given in equation (5.4),

$$\mathcal{F}_c[\dot{\kappa}(x,z):x\to\eta]\propto N(\eta,z). \tag{5.56}$$

The Hankel-transformed electron number density N can therefore be approximated by sampling $\dot{\kappa}$ at several values of x and then applying a discrete Fourier transform. Let the function G be defined as

$$G(\eta)=\frac{\mathcal{F}_c[\dot{\kappa}(x,z_1):x\to\eta]}{\mathcal{F}_c[\dot{\kappa}(x,z_2):x\to\eta]}=\frac{N(\eta,z_1)}{N(\eta,z_2)}. \tag{5.57}$$

Use of the approximation in equation (5.43) shows that

$$G(\eta)\sim\exp\left[\left(\lambda-u_0-\frac{D\eta^2}{2D_L u_0}\right)(z_1-z_2)\right]. \tag{5.58}$$

The parameters λ - u_0 and $D/D_L u_0$ can therefore be determined by evaluating G from measurements of $\dot{\kappa}$ at two values of z and then fitting a Gaussian to the result. These parameters can be cast in a more familiar form by use of equation (5.18). This gives

$$\lambda-u_0=\lambda\left(1-\sqrt{1-4\alpha_i D_L/w}\right); \tag{5.59}$$

for $\alpha_i D_L << w$ this reduces to

$$\lambda-u_0\sim\alpha_i(1+\alpha_i D_L/w). \tag{5.60}$$

In the same limit,

$$\frac{D}{D_L u_0}\sim\frac{2D}{w}\left(1+\frac{2\alpha_i D_L}{w}\right). \tag{5.61}$$

Note that

$$\dot{\kappa}(0,z)=2w\alpha_i\sigma\int_0^\infty N(\eta,z)\,d\eta. \tag{5.62}$$

The parameter u_0 can therefore be estimated by fitting the integral in this equation to samples of $\dot{\kappa}$ taken near the anode.

It can therefore be seen that the techniques described above permit the determination of α_i and the ratios w/D_L and D/D_L in a discharge in which the distribution and size of the cathode current are unknown. However, it does not appear to be possible to deduce the value of w using steady-state measurements.